Rao *et al.*
Journal of Engineering and Applied Science (2022) 69:79
https://doi.org/10.1186/s44147-022-00127-y

Journal of Engineering and Applied Science

REVIEWS Open Access

Synthesis, stability, and emission analysis of magnetite nanoparticle-based biofuels

M. Srinivasa Rao[1*], Ch. Srinivasa Rao[2] and A. Swarna Kumari[3]

*Correspondence:
srinivas.m340@gmail.com

[1] Research Scholar, Department of Mechanical Engineering, JNTUK, Kakinada, Andhra Pradesh, India
[2] Department of Mechanical Engineering, KHIT, Guntur, Andhra Pradesh, India
[3] Department of Mechanical Engineering, UCEK, JNTUK, Kakinada, Andhra Pradesh, India

Abstract

In recent years, the application of nanoadditives in biofuels is gaining much attention due to their increase in thermophysical properties such as high surface area, thermal conductivity, and mass diffusivity. However, lack of stability, high additive cost, and difficult recovery from engine exhaust are the high-priority and demanding characteristics, which may be chosen by many researchers. In this regard, the most promising nanoadditives are magnetite nanoparticles, having a high-specific area, strong magnetic response, control over the particle size and, most importantly, easy and rapid separation from exhaust gas by applying external magnetic bars. Moreover, it can be easily diluted into biodiesel, and thus, it can collect the advantages of biodiesel in water emulsion. From the literature survey, it is found that there is a lacuna in the synthesis and performance of magnetite nanofuels for internal combustion engine applications. Thus, the present study aims to epitomize the research findings related to the synthesis, characterization, stability, and properties of biodiesel/diesel-based fuels blended with magnetite nanoparticles and the influence of the magnetite nanofuels on engine performance. The study shows that the addition of nanoparticles to biodiesel has positive effects in reducing harmful emissions such as carbon black, smoke opacity and NO_X, with improved thermal efficiency and fuel consumption.

Keywords: Magnetic nanocatalyst, Co-precipitation method, Sol–gel method, Characterization methods, Stability analysis, Diesel engine performance, Engine emissions

Introduction

Emissions from vehicles have transformed into a dangerous issue for the whole world since they contribute to a huge role in air contamination. In this manner, research is being developed to reduce or trap these non-combustible particles to release them into the atmosphere. To determine these issues, analysts have proposed a couple of procedures, such as adding fuel additives and utilizing hybrid fuels, that might result in bringing about greater engine performance and lower emission characteristics [1]. Recent studies have proven the capability of nanoparticles to be utilized as an innovative fuel additive to improve engine performance and emission characteristics [2–7]. In the global context of stringent emission regulation, diesel engine emissions continue to be a subject to increasingly stringent standards.

Springer Open

© The Author(s) 2022. **Open Access** This article is licensed under a Creative Commons Attribution 4.0 International License, which permits use, sharing, adaptation, distribution and reproduction in any medium or format, as long as you give appropriate credit to the original author(s) and the source, provide a link to the Creative Commons licence, and indicate if changes were made. The images or other third party material in this article are included in the article's Creative Commons licence, unless indicated otherwise in a credit line to the material. If material is not included in the article's Creative Commons licence and your intended use is not permitted by statutory regulation or exceeds the permitted use, you will need to obtain permission directly from the copyright holder. To view a copy of this licence, visit http://creativecommons.org/licenses/by/4.0/. The Creative Commons Public Domain Dedication waiver (http://creativecommons.org/publicdomain/zero/1.0/) applies to the data made available in this article, unless otherwise stated in a credit line to the data.

Several researchers [8–10] have attempted to improve the fuel properties by introducing various nanoadditives into the fuel mixture. These nanoadditives have been shown to be helpful in improving combustion efficiency and reducing emission levels. Metal-added substances such as iron, copper, aluminum, silver, titanium, cerium, zinc, etc., have been analyzed completely for combustion behavior, engine performance, and emission characteristics. Most of the investigations have a general consensus that nanosized metal additives improve the catalytic activity during combustion, promote complete and efficient combustion, and ultimately lead to good overall engine performance. Despite the various advantages of incorporating nanoparticles into liquids, a major issue is the stability analysis of nanofluids and the arrival of nanoparticles into the environment. Some of the examinations have shown that settlement of nanoparticles decreases the fuel properties, which in turn decreases the engine characteristics and also increases the possibility of a clogged fuel injection system. To reduce the settling of nanoparticles in the base fuel, several techniques such as addition of surfactant, appropriate stirring, and proper selection of nanoparticles should be done [11–14].

The idea of adding magnetite nanoparticles is that it exhibits a fluid-magnetic coupling behavior where the fluid's position can be controlled by an applied magnetic field and also discharges extra heat over the span of the ignition interaction. Moreover, it can easily be diluted into biodiesel, and thus, it can collect the advantages of water-biodiesel emulsions. Therefore, it is well known that the researchers took advantage of utilizing magnetite nanoparticles in diesel and biodiesel mixtures and also the feature of gathering particles from the exhaust gas. To date, numerous review papers on the synthesis, characterization, and application of magnetite nanoparticles in various fields have been published. However, up to now, the published reviews do not highlight the details of reaction parameters in the synthesis and usage of nanoadditives with various fuels in IC engine applications. Most of the reviews only discuss the synthesis of nanoparticles in general without focusing specifically on the reaction parameters of magnetite nanoparticles. Hence, in this review, we will focus on the mechanism, process, and reaction parameters of two chemical synthetic methods, namely co-precipitation and sol–gel synthesis, and also the characterization and performance of magnetite nanoparticles blended biodiesel for I.C. engine applications.

Global magnetite nanoparticle market by applications

In recent times, the global market of magnetite nanoparticles has increased due to more usage of nanoparticles in various sectors such as electronics, bio-medical [15–19], energy, and waste treatment [20–22], which were shown in Figs. 1 and 2. According to a Marker Research Future Reports (MRFR) study, this market will grow at a CAGR of 10.8% by the end of 2026. At room temperature, these nanoparticles have super magnetic characteristics and can be controlled with a magnetic field. Because of the predicted growth in affordable healthcare plans, increased life expectancy, and an increase in the number of life-threatening chronic disorders, these nanoparticles have sparked significant interest in the biomedical application industry. Scientists are looking at ways to employ magnetite nanoparticles as a drug delivery agent and to improve cancer therapy efficacy. Furthermore, due to the rising penetration of items such as spintronics, nanowires, and quantum dots, these magnetite nanoparticles are becoming increasingly

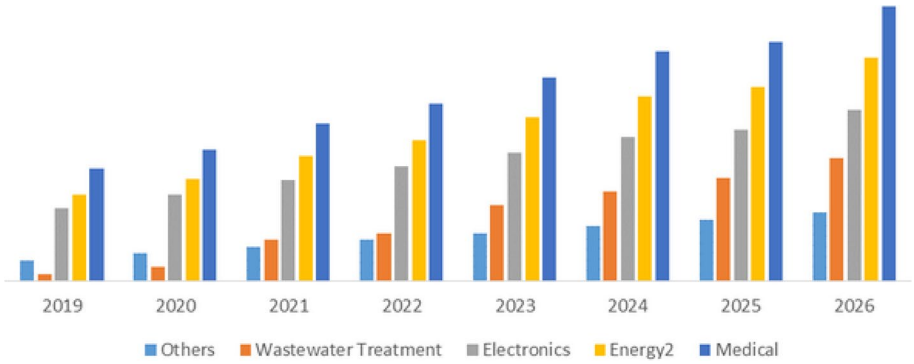

Fig. 1 Global magnetite nanoparticles market by application 2019–2026 (USD million). https://www.maximizemarketresearch.com

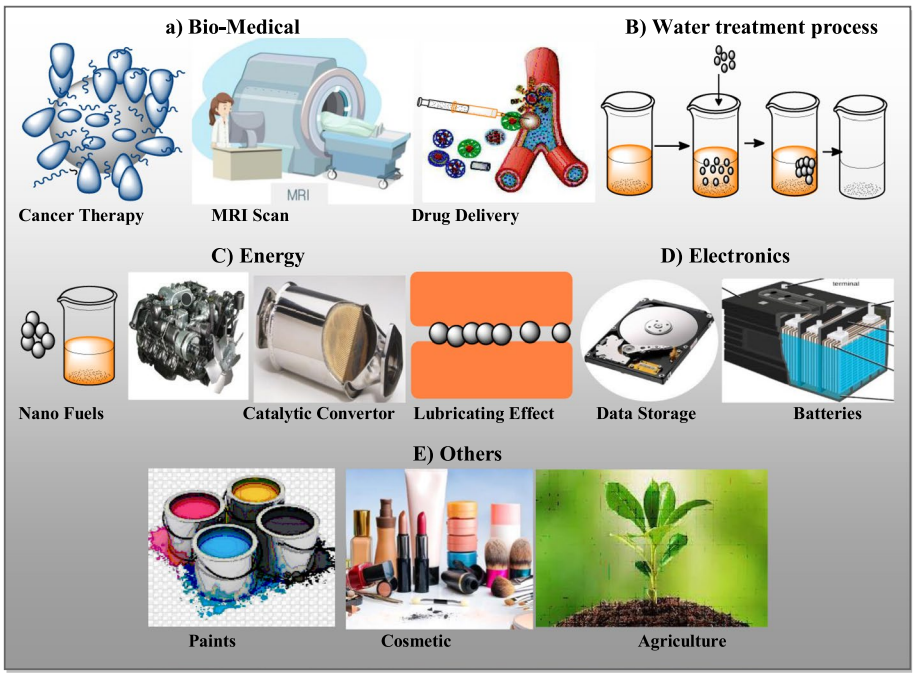

Fig. 2 Applications of magnetite nanoparticles in various sectors

attractive in the nanoelectronics industry. However, the energy sector accounted for a large sale share in 2018 because of the rising application of the product in fuel cells, batteries, and solar film coatings.

Application of nano in agriculture and catalytic convertor

Agriculture

Nano-derived agricultural products play a pivotal role in improving plant development and crop output. According to researchers, iron oxide nanoparticles are often used in rooting substrate (nutrient solution/sand/soil) as well as seed treatment, like as fertilizers. According to Zhu et al. [23], implementing iron oxide nanoparticles through the nutritional solution approach was highly beneficial for the growth and development of

pumpkin and lima beans. Mengmeng et al. [24] investigated the capacity of iron oxide nanoparticles to replace traditional Fe fertilizers as a fertilizer, and their findings indicated that Fe_2O_3 nanoparticles increased root length, plant height, and biomass values in peanut plants. Roghayyeh et al. [25] explored the yield and growth of soybean when different iron oxide doses (0, 0.25, 0.5, 0.75, and 1 g/L) are used, and the outcomes revealed that 0.75 g/L enhanced leaf + pod dry weight and pod dry weight. The maximum grain yield was obtained when 0.5 g/L nano-iron oxide was used, which resulted in a 48% increase in grain production when compared to the control.

Catalytic convertor

A catalytic converter is a device that reduces the toxicity of internal combustion engine pollutants. A catalytic converter generates an atmosphere for a chemical process that transforms dangerous combustion byproducts into less toxic compounds. Zhiqing et al. [26] observe that Fe_2O_3 catalyst exhibits excellent activity in the reduction of nitrogen oxides, and the author also mentions ANCF catalytic that can improve engine emission and combustion characteristics, thereby reducing energy and environmental problems caused by traditional fuel combustion. Syed et al. [27] created a low-cost three-way catalytic converter coated with aluminium oxide nanoparticles as a catalyst, and the author discovered that the conversion efficiencies of Al_2O_3-based catalytic converters are 99.5% for CO emissions and 92% for HC emissions, respectively. Songül et al. [28] created a catalytic converter with an $Al_2O_3/SiO_2/TiO_2$-coated catalyst that reduced exhaust emissions significantly, with a maximum reduction of 43.05% NO_X emissions at 75% load, 56.84% HC, and CO emissions at 25% load and 66.7% at 25% load.

Methods for preparing magnetite nanoparticles

Different magnetite nanoparticles can be synthesized by different techniques like co-precipitation [29–33], hydrothermal [34], thermal decomposition [35–37], and sol–gel [38, 39]. These technologies have the potential to be beneficial in the preparation of various forms of Fe_3O_4. The co-precipitation and sol–gel methods are the most extensively utilized for the synthesis of nanoparticles. In these methods, the desired shape and size of nanopowder are obtained by considering pH, reaction temperature, reaction time, and concentration of the initial solution. The co-precipitation method is the most well-known and widely used chemical method for producing nanoscale Fe_3O_4 [40, 41]. The process requires mixing of iron(III) and iron(II) particles in a strong basic solution at ambient temperature or high temperature at a molar ratio of 1:2 [42, 43]. The molecular size and shape of the magnetite nanoparticle can be determined via changing the proportion of iron salts (like chlorides, sulfates, nitrates), reaction temperature, pH value, medium ionic strength, and other reaction parameters (for example, stirring speed, basic solution-dropping speed) [44–46]. This section summarizes the two most common methods for producing magnetite nanoparticles, namely co-precipitation and sol–gel techniques, as shown in Fig. 3.

Co-precipitation method

The co-precipitation technique is a strategy for the synthesis of magnetite nanoparticles which is easy to do with an achievement rate of 96 to 99.9% [47]. Iron oxide nanoparticles

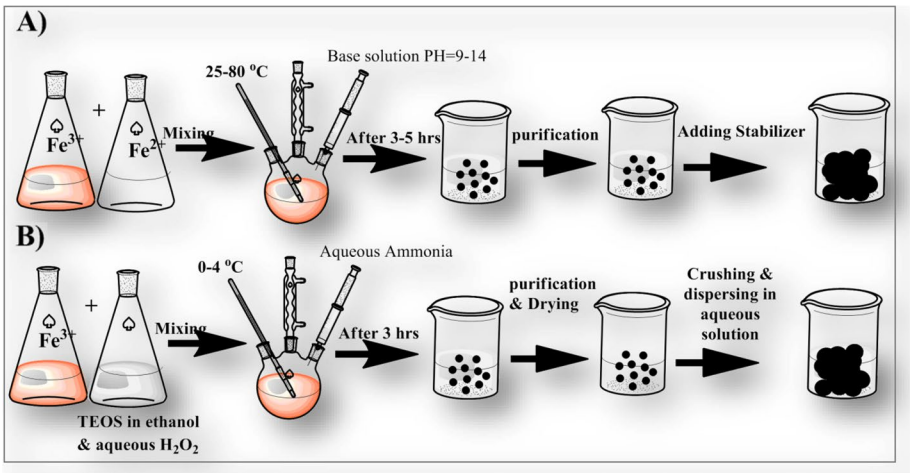

Fig. 3 Chemical methods of magnetite nanoparticle synthesis **A** co-precipitation method and **B** sol–gel methods

are prepared using this technique by adding Fe(II) and Fe(III) aqueous solutions to the base solution under anaerobic conditions at atmospheric or high temperatures [48]. However, certain factors such as salt type, reaction temperature, solution pH, Fe(II): Fe(III) proportion, and ionic strength of the mixture all have a distinct influence on the molecular size and shape of the appealing Fe_2O_3 nanoparticles [49]. The chemical formation of magnetite nanoparticles by co-precipitation methods is shown in Eq. 1 [50].

$$\mathbf{Fe^{2+} + 2Fe^{3+} + 8OH^{-} \rightarrow Fe\,(OH)_2 + 2Fe\,(OH)_3 \rightarrow Fe_3O_4 + 4H_2O} \quad (1)$$

Kumar et al. [51] utilize two solutions of ferric nitrate salt and sodium hydroxide in a 1:2 mole proportion with distilled water that are thoroughly mixed and sonicated for 60 min. The completed homogeneous solution is then calcined up to 350°C to take out moisture and achieve crystallization. The particle's average diameter was computed and viewed as about 30 nm. Wu et al. [48] utilized ferrous sulphate hexahydrate as the starting material to create magnetite nanoparticles by co-precipitation. The molar proportion of Fe^{3+} and Fe^{2+} in the $FeCl_3$ arrangement was changed in accordance with 1.5:1 by adding a measured amount of $FeSO_4.7H_2O$. With ultrasonic agitation, sodium hydroxide (NaOH) was added, bringing about a black solid. The resultant Fe_3O_4 precipitate was warmed in an ultrasonic water bath for a half-hour at 65°C.To refine the molecule, the created Fe_3O_4 samples were washed a few times with ethanol and deionized water. The particles were then vacuum-dried at 74°C. Radwan et al. [52] utilized $FeCl_3$ and $FeCl_2$ combinations were treated with distilled water before adding 1.5M NaOH drop-wise with vigorous stirring to create a dark-black precipitate. The solution was decanted, and the resultant Fe_3O_4 sample was washed multiple times with distilled water before being rinsed with $(CH_3)_2CO$ and dried for 5 h at 80°C in a heater. Following drying, the sample size was decreased to the most reduced molecule size achievable and characterization was performed as needed. Karthikeyan et al. [53] likewise utilize the mixing of $FeCl_3$ and $FeCl_2$ in a funnel-shaped jar containing 25 ml of 0.4 N hydrochloric acid. Then, at that point, 200 µl of $C_{18}H_{34}O_2$ was mixed in with 3 ml of $(CH_3)_2CO$. From that point on,

250 ml of 1.5 N sodium hydroxide solutions is added drop-wise while stirring. To help the process, 100 µl of oleic acid was added in 10-min increments. This brought about a dark color. The nanoparticle development in the precursor was permitted to continue for 30 min with steady stirring. At last, a single layer of surfactant-coated magnetite nanoparticles was formed subsequent to the chilling, continued washing, centrifugation, and decantation. Aliramaji et al. [54] produced magnetite nanoparticles by dissolving $FeCl_2.4H_20$ and $FeCl_3.6H_20$ in 60ml of HCl. This solution was then added drop by drop to a 100-ml NaOH solution, mechanically stirred at 1000rpm and in an ultrasonic bath. After the magnetite black precipitate was obtained, it was mechanically stirred and put in an ultrasonic bath for 1/2 h. A permanent magnet was utilized to separate the precipitate, which was then washed with distilled water. Lazhen et al. [55] made magnetite nanoparticles by dissolving 2.8 and 4.0 g of $FeSO_47H_2O$ and $Fe_2(SO_4)_3$ in distilled water of 100 ml for 5 min with a magnetic stirrer. Under stirring, different amounts of sodium dodecyl sulphate were added to this mixture. By stirring, the pH value was adjusted to 12 for 20 min at room temperature with solid NaOH. The frequency of visible light (400–750nm) was set at a decent distance of 10cm. The black precipitates were created and flushed many times with C_2H_5OH and distilled water until the pH reached neutral. Finally, magnetite nanoparticles were obtained by drying the resulting dark precipitates in air at room temperature. Ahmad et al. [56] also produce magnetite nanoparticles by dissolving $FeCl_3.6H_2O$ and $FeCl_2.4H_2O$ with a 2:1 mole proportion in 100 ml aquades, then, at that point, mixing the two solutions in a 500-ml beaker glass and warming for 10 min while stirring. After warming, 20 ml of NH_4OH was progressively added while the solution was aggressively agitated with a magnetic stirrer at 300, 400, and 500 rpm until the pH arrived at 10. Then, at that point, at temperatures of 40°C, 60°C, and 80°C, heat continuously for 30 min. Fluid and precipitate were then separated using filter paper and washed with aquades. The precipitate was dried in an air oven for 150 min at 100°C. Tables 1 and 2 show a brief summary of magnetite nanoparticle synthesis using an ultrasonicator and mechanical stirrer.

Sol–gel method

One more excellent synthetic methodology for creating magnetite nanoparticles is the sol–gel strategy [81, 82]. It includes changing over discrete particles (sol) into a three-dimensional polymeric organization by hydrolysis of precursors into a stable colloidal arrangement (gel). The gelation cycle can be reversible (for electrostatic contacts or hydrogen bonds) or irreversible (for covalent bonds) depending on the nature of interactions between colloidal particles [83]. The gel is then dried or warmed to create the nanomaterial [84]. Equations 2 and 3 [85] show the chemical formation of magnetite nanoparticles using sol–gel methods.

$$\boldsymbol{Fe^{3+} + \ 3H_2O \rightarrow (OH)_3 + 3H^+} \tag{2}$$

$$\boldsymbol{12(OH)_3 \rightarrow 4Fe_3O_4 + 18H_2O + O_2} \tag{3}$$

Shaker et al. [86] dissolved $Fe(NO_3)_3$ and $C_2H_6O_2$ in the appropriate concentrations and agitated for 120 min at 400°C. The produced mixture was then warmed to 800°C to generate brown gel. After that, the gel was matured at room temperature for

Table 1 Summary of magnetite nanoparticles synthesis by co-precipitation method using Ultrasonicator

Precursors	Precipitating Agent	Reaction conditions	Particle Size (nm)	Ref
1.9g $FeCl_2$ $4H_2O$ & 5.4 g $FeCl_3$ $6H_2O$	6 ml of NH_4OH	Room temp. for 30 min	216 ± 0.5	[57]
1.5:1 M $FeCl_3$& $FeSO_4.7H_2O$	NaOH	65°C for 30 min	_	[58]
1.5 mmol $FeCl_2 4H_2O$ & 3 mmol $FeCl_3 6H_2O$	10 ml NH_4OH	40°C	7	[59]
1:2M $FeSO_4$ $7H_2O$ and $FeCl_3$	3.2g NaOH	55°C	12.2 - 2.9	[60]
1.5:1M $FeCl_3$ and $FeSO_4$ $7H_2O$	NaOH	65°C for 30 min	15	[48]
2M $FeCl_2$ $4H_2O$ and 3M $FeCl_3$ $6H_2O$	0.3 mol NH_4OH	50°C for 30 min	11.4	[61]
$FeCl_2$ $4H_2O$ and $FeCl_3$ $6H_2O$	1M NaOH	30 min	_	[54]
1:2 M $FeCl_2$ $4H_2O$ & $FeCl_3$ $6H_2O$	NaOH	sonication	_	[62]
2.17g $FeCl_2$& 3.01g $FeCl_3$	16.8 g KOH	stirring 300 rpm & 90°C	8.19	[63]
		sonication 10 kHz for 60 min	8.01	
1.5:1M $FeCl_3{\cdot}6H_2O$ & $FeSO_4{\cdot}7H_2O$	3.5M NH_4OH	Stirring and mixing at 50°C	15.6	[64]
		sonication	14.6	

approximately 60 min before being annealed in a heater under an air environment at 200, 300, and 400°C. Finally, magnetite nanoparticles of different sizes were made. Suhel et al. [87] use 0.2 and 0.1 moles of $FeCl_3$ and $FeSO_4.7H_2O$ solutions in distilled water, which are gently stirred at 500 rpm in a magnetic stirrer at room temperature while the ferric chloride solution is added. From that point forward, drop by drop of hydrochloric (HCL) acid is added while stirring, and the mixture is left at 50°C for 30 min. At 10 PH, ammonia is added to the solution, and the mixture is changed over to dark, revealing the production of absolute nanoparticles. After that, the gel is allowed to dry in an oven at 80°C for 120 min before being calcined in a heater at 200°C for 120 min. The calcined gel was manually mashed using a crusher and pestle. Takai et al. [82] utilize a 2.35g of $FeCl_3.6H_2O$ and 8.35g of $FeCl_2.4H_2O$ were dissolved in 60 ml of ethylene glycol and rapidly agitated for 3 h at 45°C. Following that, the solution was warmed and kept at an 80°C temperature till a dark colored gel formed. This gel was matured for 72 h before being dried at 140°C for 5 h. The resulting xerogel was vacuum-annealed at temperatures ranging from 200 to 400°C. At long last, magnetite nanoparticles of different sizes were successfully created. Table 3 shows a brief summary of magnetite nanoparticle synthesis using the sol–gel method.

Characterization of magnetite nanoparticles

Once the magnetite nanoparticles were synthesized, they needed to be characterized in order to evaluate their shape, molecule size, size distribution, composition, and magnetic characteristics. In this section, we will go through the different techniques for determining the physical and chemical characteristics of these nanoparticles, which were shown in Figs. 4, 5, and 6 [85–98, 105].

The scanning electron microscopy (SEM) method gives a direct assessment of nanotubes arrangement and size. Veeradate et al. [84] utilize SEM to examine the morphology of nanoparticles. The SEM images show that the majority of the

Table 2 Summary of magnetite nanoparticles synthesis by co-precipitation method using mechanical stirrer

Precursors	Precipitating Agent	Reaction conditions	Particle Size (nm)	Ref
0.75g $FeCl_2$ $4H_2O$ & 1.75g $Fe(NO_3)_3$ $6H_2O$	5.5 ml NH_4OH	Stirring by 500 rpm	13±1	[65]
1.625g $FeCl_2$ $4H_2O$ & 4.430g $FeCl_3.6H_2O$	10 ml NH_4OH	Stirring by 1000 rpm for 2h at 25 °C		[66]
10 & 20 mmol/L $FeCl_3$ $FeCl_2$	1 M NaOH	_	3 to 5	[67]
1:2 M $FeCl_2.4H_2O$ & $FeCl_3.6H_2O$	NaOH	_	10.56	[68]
17.15g $FeSO_4{\cdot}7H_2O$ & 35.5 ml $FeCl_3$	20.7g NaOH	_	10–50	[69]
25mM $FeCl_2$& 50mM ferrous nitrate	NaOH, KOH, NH_4OH	Stirring for 1 h at 25°C	11.23±2.04	[70]
		Stirring for 1 h at 50°C	9.01±1.30	
		Stirring for 1 h at 70°C	6.83±1.11	
5.2g of $FeCl_3$& 4.448g $FeSO_4{\cdot}7H_2O$	1.5 M NaOH	Stirring by 600 rpm at room temperature	86.01	[71]
6.5g of $FeCl_3$& 5.56g $FeSO_4.7H_2O$	1.5 M NaOH	Stirring by 600 rpm with heating at 80°C	74.14	
1.99g $FeCl_2.4H_20$ & 5.41g $FeCl_3.6H_2O$	25% $NH_3.H_2O$	Stirring at 25°C,40°C,60°C,80°C for 60 min	10.14±0.2 10.32±0.9 10.95±0.8 11.66±0.87	[72]
$FeCl_2.4H_2O$ & $FeCl_3.6H_2O$	35 ml NaOH	stirring by 200 rpm at 25 °C	10.03	[73]
$FeCl_2.4H_2O$ & $Fe_2(SO_4)_3$			6.6	
$FeCl_2.4H_2O$ & $Fe(NO_3)_3.9H_2O$			8.86	
$FeSO_4.7H_2O$ & $FeCl_3.6H_2O$			8.7	
$FeSO_4.7H_2O$ & $Fe_2(SO_4)_3$			5.1	
$FeSO_4.7H_2O$ & $Fe(NO_3)_3.9H_2O$			8.23	
8.64g $FeCl_2$ $4H_2O$ & 23.50g of $FeCl_3$ $6H_2O$	34.4 ml NH_4OH	Stirring by 300 rpm & heating at 60°C	20-78	[74]
0.01M $FeCl_2{\cdot}4H_2O$ & 0.02M $FeCl_3{\cdot}6H_2O$	0.08-0.1 M NaOH	Stirring at 500 rpm	10.7-11.5	[75]
	0.09 KOH		7.1	
16.25g $FeCl_3$& 6.35 g of $FeCl_2$	2 M NaOH	Stirring at 30°C	_	[76]
1.5 g of $FeCl_2$ $4H_2O$ & 3.0 g of $FeCl_3$	10 ml NH_4OH	Stirring at various temps. (0–90°C)	10–40	[77]
2:1M $FeCl_2$ $4H_2O$ & $FeCl_3{\cdot}6H_2O$	3M NaOH	Stirring for 30 min	12.6-13.8	[78]
0.01 M $FeCl_2.4H_2O$ & 0.02 M $FeCl_3.6H_2O$	1.5M NaOH	_	10 to 13	[79]
1M $(NH_4)_2Fe(SO_4)_2$& 2M $FeCl_3$	0.5M NaOH	Stirring & kept at 80°C	20	[80]
1M $FeCl_2{\cdot}4H_2O$ and 2M $FeCl_3{\cdot}6H_2O$	20 ml NH_4OH	Stirring by 300, 400, and 500 rpm	_	[56]

nanoparticles have a circular shape with a molecule size of 100nm, which is obtained from the ablated laser energies. Besides, it was seen that the molecule size developed with an increase in laser energy. Syed et al. [106] utilize electron microscopy to investigate the morphological and surface characterization of iron oxide nanoparticles. It was noticed that spherical shaped iron oxide nanoparticles were obtained and the diameter dispersion ranged from 24 to 65nm. Nouri et al. [104] utilized transmission electron microscopy (TEM) and SEM to look at the size and form of nanoparticles, confirming that the size of the nanoparticles was 20–40nm. Shafii et al. [102] noticed the size and shape of nanoparticles utilizing TEM examination. The average molecule diameter is around 10nm, which is consistent with expectations. Kulkarni et al. [101]

Table 3 Summary of magnetite nanoparticles synthesis by Sol-Gel method

Precursors	Annealing temp. (°C)	Particle size (nm)	Ref
2.35g of Fe (III) and 8.35g of Fe (II) dissolved in 60 ml of ethylene glycol	200	2.02	[82]
	300	5.58	
	400	8.35	
2.70g of $FeCl_3{\cdot}6H_2O$ and 0.995g of $FeCl_2{\cdot}4H_2O$ dissolved in 10ml ethanol	250-400	9~12nm	[88]
Ferric Nitrate dissolved in ethylene glycol	200	28.9	[87]
	300	88.7	
	400	67.6	
6 g of Iron (III) acetylacetonate dissolved in a 36 ml methanol.	_	8	[89]
0.2M of ferric nitrate in ethylene glycol	200	7.8	[90]
1M of ferric nitrate in ethylene glycol		13.8	
0.2 mol of ferric nitrate dissolved in 100 ml ethylene glycol	200–400	18	[91]
Ferric Nitrate dissolved in ethylene glycol	500	50	[92]
0.2 M dehydrated ferric chloride and 0.1 M hydrated ferrous sulphate	200	18.21	[87]
1:2 ratio of iron nitrate and citric acid were dissolved in distilled water	400	10-18	[93]
4.04g Ferric Nitrate dissolved in 50 ml ethylene glycol	400	20-40	[94]
16.159 g of ferric nitrate dissolved in 25 ml of ethylene glycol	250	18.46	[95]
	300	27.68	
1:0.8 M of Ferric nitrate and citric acid dissolved in 113ml of deionized water	450	3-20	[96]
32.3 mg of iron nitrate dissolve in 30 ml of ethylene glycol	300		[97]
14 g of iron (III) nitrate dissolved in 55 g of ethylene glycol	300	15 nm	[98]

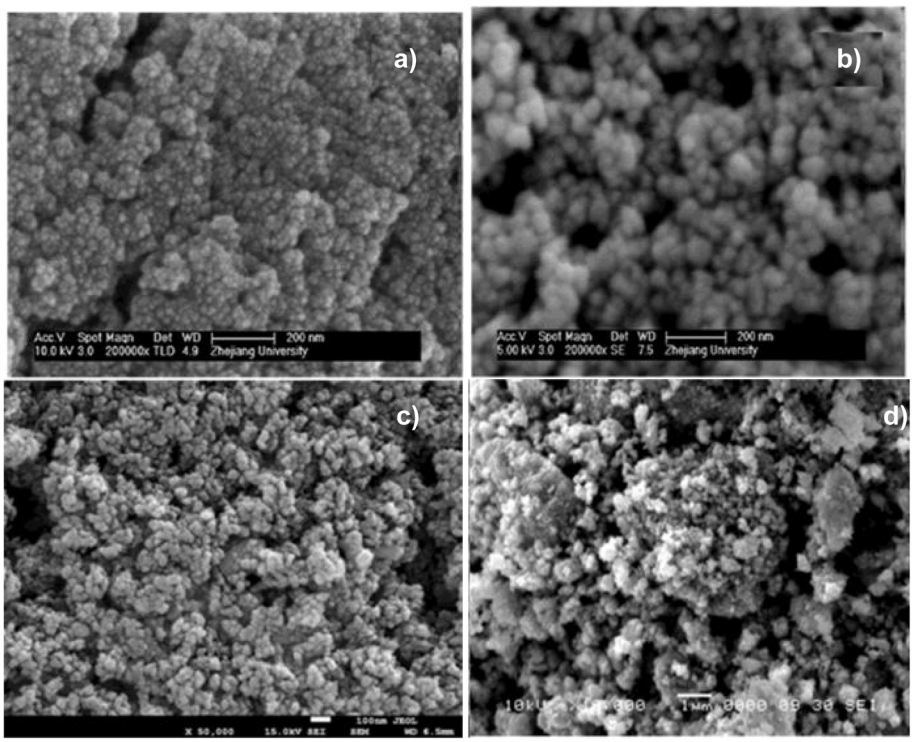

Fig. 4 SEM analyses of various size nano particles **A** spherical shape and average size about 12nm at 200oC [99], **B** spherical shape and average size about 53nm at 250oC [99], **B** spherical shape and size less than 100 nm [100], and **D** spherical shape and size varies from 24 to 65 nm [101]

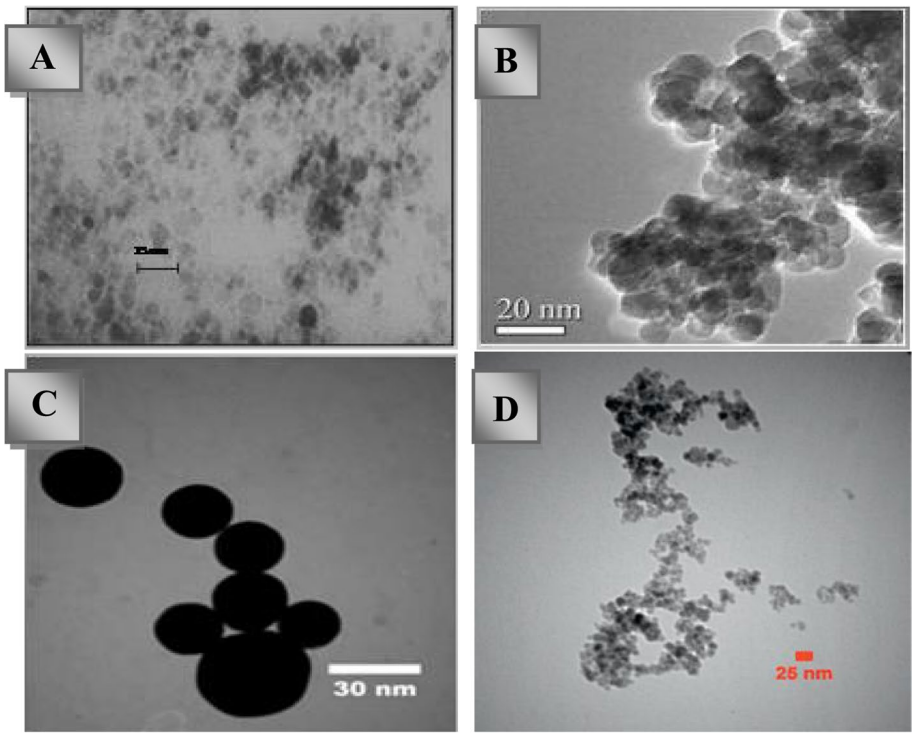

Fig. 5 TEM analyses of various size nano particles. **A** Average size is 10 nm [102], **B** 20 nm [103], and **C** 20–40 nm [104], and **D** spherical and size of the particles are approximately 10–12 [54]

utilize a coprecipitation strategy to make magnetite nanoparticles and were characterized using X-ray diffraction (XRD) examination and scanning electron microscopy. According to these two techniques, homogenous-sized magnetite nanoparticles with a spherical form may be created. The SEM of magnetite nanoparticles shows a spherical structure with a diameter of around 10–15 nm, which agrees with the XRD information. The X-ray diffraction technique is utilized to find out the oxygen content, purity, and crystalline structure [98]. Suhel et al. [87] examined X-ray patterns with a 0.05 step size at 2ɵ angle (20⁻70º), revealing that the patterns of produced magnetite nanoparticles had a cubic structure. Moreover, magnetite nanoparticles were viewed as being of high purity and crystalline in this review. Following that, TEM is utilized to determine the shape and molecule size of magnetite nanoparticles. The two magnifications of the TEM images revealed that the molecules have a spherical shape. The author also shows the molecular size distribution histogram plotted from the diameters of 70 nanoparticles. According to the histogram, the mean crystal size is 1.81nm with a standard deviation of 1.8nm. On the other hand, Debye Scherer's formula gives an average crystal size of 18.21 nm. This difference in crystal size shows a variation in size from 11 to 20nm. P. OU et al. [99] synthesized magnetite nanoparticles using a solvothermal technique and analyzed them using SEM at 200 and 250°C for 24 h, respectively. The powder is comprised of homogeneous spherical nanoparticles with a diameter of around 12 nm on average. When the solvothermal temperature was raised to 250°C, however, significant variations in the diameter of magnetite crystallites with a size of roughly 53nm were noticed.

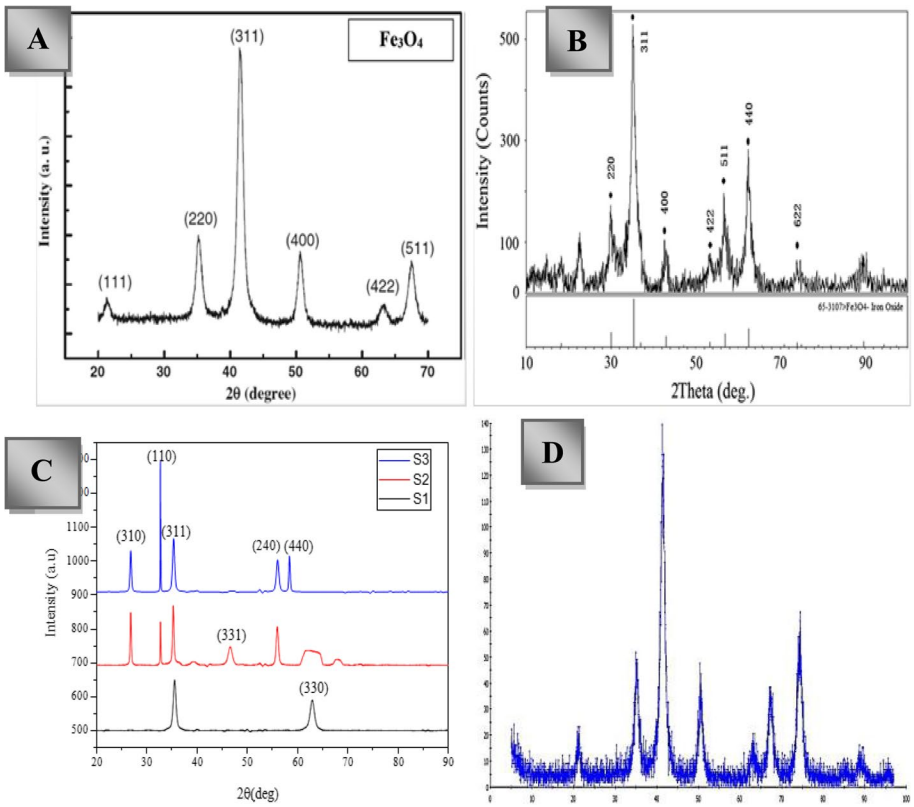

Fig. 6 XRD analyses of magnetite nanoparticles. **A** Highly crystalline and average particle size were 18.21nm [103]. **B** Highly crystalline and average particle size were 19.4nm [48]. **C** Average particle sizes were 2.02nm, 5.58nm, and 8.35nm [82]. **D** Crystalline and average particle sizes were 16nm [54]

Preparation of magnetite nanofuels

To make a homogeneous magnetite nanofuel, techniques like ultra-sonication, pH adjustment, and magnetic stirring are performed [107]. To improve the thermal agitation of these nanoparticles, numerous ultra-sonication procedures, including probe-type and bath-type, are applied [108]. Magnetic stirring is best for lower concentrations of magnetite nanoparticles in the vessels containing fluids driven by a rotating fixed electromagnet or a couple of turning electromagnets attached underneath the mixing device. The PH modification approach depends on changing the pH value of nanofluids in order to improve the mixing dispersion. In practice, a combination of one of the aforementioned dispersion methods (i.e., ultra-sonication, magnetic stirring, and pH modification) is commonly used to provide improved efficiency and stability.

Suhel et al. [87] have prepared magnetite nanofuel by mixing 20% chicken fat methyl ester (CFME) and 80% pure diesel with different dosages of 50, 100, and 150 ppm. In this experiment, the author uses the titanium horn test ultrasonicator for the suspension of magnetite nanoparticles for 45 min at 40°C with a frequency of 20 kHz. This sonicator scatters the particles equally, which prevents agglomeration [53] create magnetic nanofuel from 98.7% algal oil methyl ester (CROME), 1% Fe_3O_4, and 0.3% $[(CH_3)_3NOH]$. For improved mixing and homogenous suspension, magnetite

nanoparticles are suspended by an ultrasonic agitator with continual agitation for an hour. The ferrofluid-altered base fuel was kept in a glass container with a stopper at room temperature for 1 month to assess the phase change characteristics. Syed et al. [106] also prepare the magnetic nanofuel by considering 1 l of diesel and afterward adding 0.025g and 0.05 g of iron(II, III) oxide nanoparticles to achieve dosage levels of 25 ppm and 50 ppm, individually. The mixture was stirred for 30 min in an ultrasonic shaker to make a uniform distribution. Yuvarajan et al. [109] utilized Mahua oil methyl ester (MOME), magnetite nanoparticles, and surfactant in a beaker and stirred with an ultrasonic agitator for 60 min. Nouri et al. [104] have used pure diesel with 30, 60, and 90 ppm of magnetite nanoparticles in the solution kept in an ultrasonic bath at a 40-kHz frequency and a temperature of 50°C. The following 2 days, there was some nanoparticle collection. Prior to its utilization in the engine, the fuel mix was homogenized by exposing it to ultrasonic waves. Figure 7 shows the preparation of nanofuel using an ultrasonicator.

Stability analysis of magnetite nanofuels

The dispersion of various nanoparticles in liquid fuels offers huge advantages in burning applications. Many methodologies for assessing the stability of nanofluids have been shown in Fig. 8. The simplest one is the sedimentation method [110, 111], where the weight or the sediment volume of the nanoparticles in the nanofluid under external force shows the indication of the stability of the characteristic nanofluid. With respect to the stability of nanofluids, authors such as Kuo et al. [112] have assessed that the size of the molecules in the colloid was small and of less weight. This reduced the occurrence of sedimentation and the chance of the molecules settling, which made for a more stable nanofluid. Yu et al. [11] have utilized a particular instrument to notice the variance in the concentration or size of the molecule size with settling time. Nanofluids are viewed as stable when the molecule size or concentration of particles remains constant. Sediment imaging captured by an in vitro nanofluid camera is a more typical method for assessing nanofluid stability. According to Saxena et al. [113], the long-term stability of nanofuel suspension is dependent on different rules, and the most critical of

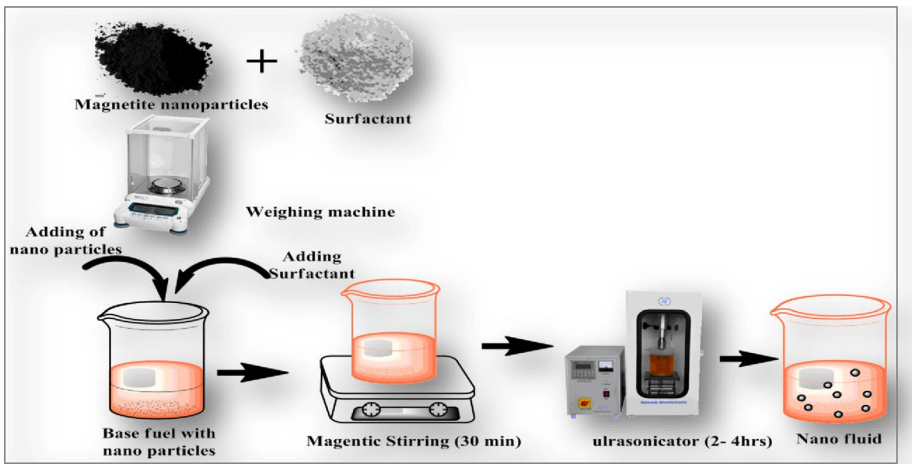

Fig. 7 Preparation of magnetite nanofluid

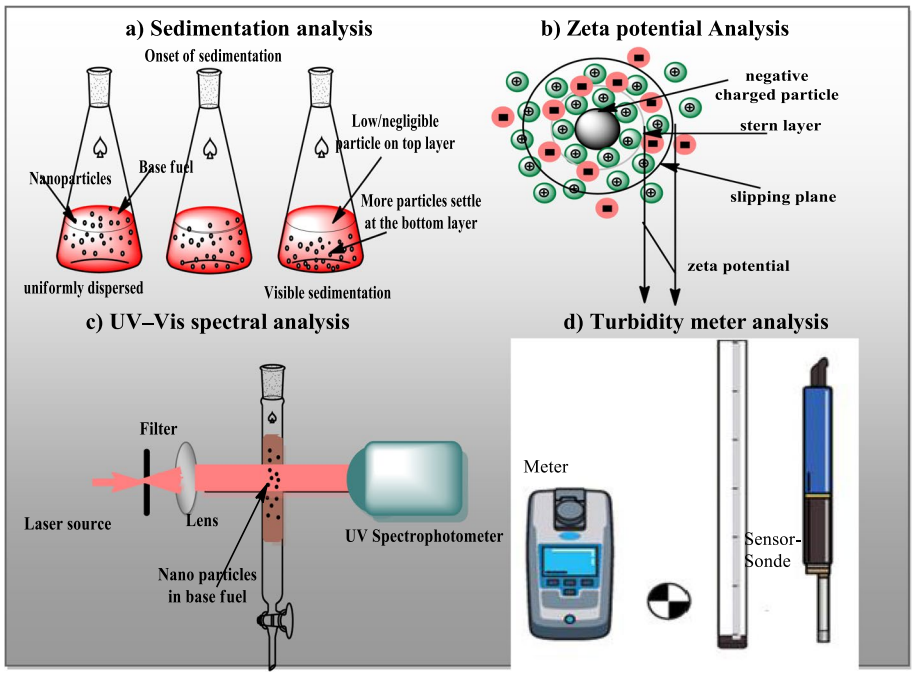

Fig. 8 Techniques for finding the stability of magnetite nanofluid

which are nanoparticle size, dose, and the synthesis process. In general, nanoparticles have less weight, which minimizes sedimentation and makes the nanofuel more stable. For settling techniques, a long observation time is the default. Therefore, a centrifugation method is performed to evaluate the stability of the nanofluid. For the sedimentation method, a long observation time is the defect. Therefore, a centrifugation method was performed to evaluate the stability of the nanofluid. Singh et al. [114] synthesized the silver nanofluid by reducing $AgNO_3$ with polyvinyl pyrrolidone (PVP) as a stabilizing agent, and the stability was tested by a centrifugation method. In this, the produced nanofluids have been shown to be stable for a month in a fixed state, and this process undergoes centrifugation at 3000 rpm for over 10 h.

Another way of evaluating the stability of nanofluids is zeta possible examination, which involves studying their electrophoretic behavior [115, 116]. According to the stabilization theory [117], if the zeta potential has a large absolute value, the electrostatic repulsions between the particles increase, bringing out good suspension stability [118]. A value of zeta potential of 20 or 25 mV can be considered as the criterion value for isolating a weakly charged surface from a strongly charged surface, and an absolute value of zeta potential of 40 to 60 mV is accepted to be stable and that a value of more than 60 mV has excellent stability [119–122]. Said et al. [123] utilized a zeta-seizer to decide the size of the nanoparticles in the base fluid as well as the value of the zeta potential. Following 30 days, a nanofluid with a high zeta capacity of 41.8 mV was created. Venkatachalapathy et al. [124] have shown that the electro-kinetic characteristics of nanofluids impact their stability. To find out the stability of the nanofluid, a zeta potential test was performed utilizing the zetasizer, giving a value of +31.4 mV, confirming the nanofluid stability. The purpose of the UV-Vis spectrophotometer [125, 126] and turbidity meter methods is to analyze the stability of the different nanofluid concentrations.

UV spectral analysis is used to find the extinction of light passing through a sample. It is a valuable tool for identifying, characterization, and studying nanomaterials due to their sensitivity to optical properties. Turbidity is also a versatile optical method similar to UV spectral analysis, used for monitoring the growth of suspended nanoparticles. Turbidity describes the clarity of a material due to the presence of particulates. The UV-Vis spectrometer determines the absorption of liquids at wavelengths from 200 to 900nm and is used to examine different dispersions in liquids [127]. Gad et al. [128] studied the UV-Vis spectroscopy of nanoparticles dispersed in diesel fuel at a concentration of 30ppm for 30 days. The wavelength of 222nm was determined to have the highest absorption. The UV absorption was raised by raising the wavelength until it arrived at its maximum wavelength of 222 nm, after which it decreased.

A turbidity meter is also another way of assessing the stability of nanofluids. In this, a light source is used to examine the nanofuel. Over an eight-week period, Balamurugan et al. [129] observed optical density decreases to 8 Nephelo turbidity units (NTU) for all samples except nanoparticles added at a rate of 10 ppm. The value of optical density value approaches 13 NTU for nanoparticles added to a sample of 10 ppm because equilibrium is formed between the surfactant monomers of the particle and the solute, resulting in effective stabilization. Seela et al. [130] study the suspension lifetime of nanosized multiwall carbon nanotubes and aluminium oxide in Jatropha methyl ester blends B20, B50, and B70. The nanofuel stability rate was determined through turbidity investigation. In more than an 18-day time frame, the rate of stability for multiwall carbon nanotubes and aluminium oxide was found to be 83.3 and 87.03%, respectively. With the 100 ppm concentration of multi-walled carbon nanotubes (MWCNT) and Al_2O_3 nanobiodiesel mixes, there was a significant decline in suspension.

Techniques for improving the stability of nanofluids

Various researchers have performed different investigations to increase the stability of nanofluids, such as ultrasonic oscillators [131, 132], addition of surfactants [133, 134], and pH control [135, 136] to accomplish optimal blending of the nanoparticles in the liquid fuel [137]. For example, there are three strategies of fluid dispersion technology; for example, medium control, mechanical control, and agent control. For molecule dispersion, the mechanical control utilizes the ultrasonic vibrator, disintegrator, and electromagnetic agitators [138].

Ultrasonic vibration

An ultrasonicator is a well-known physical methodology for dispersing agglomerated nanoparticles in the base fluid. Many examinations utilize a probe and a bath sonicator to equally scatter the nanoparticles [139–141]. Typically, ultrasonication is performed at different powers and frequencies for varying lengths of time. The duration required for sonication might be impacted by the molecule size and shape, the mixing proportion of nanoparticles, and the production process [11].

Hong et al. [142] show that longer sonication times can improve the stability of nanofluids. It was also revealed that increasing the sonication period helps to prevent the agglomeration of the particles. Amrollahi et al. [143] also reported similar examinations that showed longer sonication periods enhanced nanoparticle stability. Chung

et al. [144] use the bath and horn sonicator for the dispersion of ZnO nanoparticles in water, in which the horn type of sonicator is more effective in terms of quicker reduction rates and greater settling rates. El-Seesy et al. [145] use an ultrasonic bath for 90 min to disperse SiO_2 nanoparticles in distilled water. The silica nanofluids remained stable for 72 h without any visible settling [132]. Longo et al. [146] have used aluminium oxide and titanium oxide nanoparticles for the nanofluid preparation. The nanoparticles were mechanically stirred in the first phase and afterward sonicated at 25 kHz. The author's observer that sonication improved the efficiency of dispersion compared with mechanical stirring and that the two nanofluids were shown to be stable for a period of 1 month. Parametthanuwat et al. [147] used an ultrasonic bath at a frequency of 43 kHz for 3 h to make Ag nanofluids. The author observed that the nanoparticles were stable for as long as 48 h. Therefore, the ultrasonicator is a fundamental methodology since its objective is to decompose clusters by utilizing the sound energy of a sonicator at different frequency levels and durations for nanofluids. In addition, the molecule size and shape, mixing ratio, concentration, particle preparation process, and base fluid type all impact the best sonication conditions [148].

Addition of surfactant/activator

Nanofluid is stabilized by adding a surfactant to the liquid to reduce surface pressure and promote immersion of the particles, thus keeping them away from speedy sedimentation. Various surfactants such as polyvinyl chloride-PVP, sodium dodecyl benzene sulfonate, hexadecyltrimethyl ammonium bromide, cetyltrimethyl ammonium bromide, polyoxyethylene, nonylphenyl ether, oleic corrosive, dodecyl trimethyl ammonium bromide, gum Arabic were reported and utilized in various kinds of nanofluids [3, 110, 119, 149–155].

Vivek et al. [155] have utilized cetyltrimethyl ammonium bromide surfactant for the preparation of Al_2O_3 nanoparticles blended nanofuel, and the fuel was tested on a compression ignition engine. By the use of CTAB surfactant, the nanoblended fuel organizes and controls particles and prevents deposition. Zhai et al. [156] used sodium dodecyl sulphate as a surfactant to improve the Al_2O_3+H_2O nanofuel stability. Tiwari et al. [157] utilized a surfactant called cetyltrimethyl ammonium bromide for stability improvement and scattering of nanofluids without changing their thermo-physical characteristics. Xia et al. [153] investigated the two surfactants, namely sodium dodecyl sulphate and PVP, in Al_2O_3 added nanofuel for dispersibility and stability. In this examination, PVP demonstrated preferred dispersibility by enhancing stability over sodium dodecyl sulphate at surfactant concentrations of 0.5, 1, and 2%. One reason for nonionic PVP's superior performance, according to the author, is its relatively long alkyl chain. Kakati et al. [158] used 0.03% sodium dodecyl sulphate to create an Al_2O_3+ water nanofluid with a volume centralization of 0.1 to 0.8% at temperatures ranging from 10 to 50°C. Accordingly, the nanofluid is stable for 4–5 days, though without surfactant nanoparticles, it sediments after 1 h of production.

PH control (surface chemical effect)

One more technique for making the nanofluid more stable is to change the pH of the solution. Wen [159] used an acid treatment on carbon nanotubes (CNT) nanofluid and

showed that the suspension was moderately stable. Graphene nanoplatelets (GNP) nanoparticles were acid-treated by suspending them in a 1:3 mixture of HNO_3 and H_2SO 4[160]. After that, the mixture is washed with DI water and dried in an oven. Finally, the GNP solution is mixed with the $Ag(NO_3)OH$ solution, which has a shelf life of 60 days. Lee et al. [127] have investigated Al_2O_3 nanoparticle added nanofluids with various pH levels. From the test information shows that at pH 1.7 nanofluids, the agglomerated molecule size drops by 18% and at pH 7.66, the agglomerated molecule size increases by 51% due to a decrease in electric repulsion force. When alumina is lowered into water, ions of the hydroxyl group form on the surface. The pH allows the necessary processes to take place. The hydroxyl groups react with the positively charged H^+ in water at lower pH values.

Most significantly, keeping the pH of the solution in the optimal range is critical since maintaining acidic and basic solutions is unsafe for personnel and the workplace. Moreover, applying these kinds of soluble and acidic solutions in industries might cause surface corrosion [161]. Many investigations used sonication and dispersant addition to achieve stability, while others utilized surface functionalization and pH modification techniques. However, the majority of research focuses on short-term stability, which can be challenging when applied in practical applications and also in commercialization. Subsequently, more research is expected to evaluate the impacts of different factors on long-term stability.

Effect of magnetite nanoparticles on improved fuel properties

One of the important aspects of determining the fuel quality and engine performance is the fuel characteristics. Recently, the addition of nanoparticles has been considered to be a beneficial strategy for improving fuel characteristics. Several studies [155, 162–172] investigated fuel characteristics by incorporating various types of nanoparticles into various diesel/biodiesel blended fuels. In addition, the quality of the blended fuel and engine performance was evaluated by examining their effects on several characteristics such as density, flash point, kinematic viscosity, caloric value, and cetane number. According to Mukul et al. [173], increasing the dosing of nanoadditives causes increases in the calorific value of the fuel. During combustion processes, the nanoparticles operate as catalysts and have a good influence on ignition qualities. Furthermore, these nanoparticles have a high specific surface area and have superior heat transport capabilities, thereby having a higher calorific value. The particles enhance momentum density, which increases fuel injection velocity into the combustion chamber and hence improves engine performance. Table 4 shows the fuel characteristics of a blended diesel and biodiesel with magnetite nanoparticles in different concentrations.

Shiva Kumar et al. [51] have assessed the impact of Pongamia methyl ester blends (B10, B20, and B30) with 0.5, 1%, and 1.5% ferrofluid on the fuel properties, engine performance, and emission characteristics of a diesel engine. The results showed that the density, kinematic viscosity, and cetane number increased slightly, but there was no significant change in flash point and calorific value. Yuvarajan et al. [177] examined that adding 1.3% magnetite to the rice bran oil methyl ester results in a 3.15% increase in kinematic viscosity and a 2°C rise in flash point and water content by 0.02% increase. Other properties, such as density and calorific value, improve by 2.96% and 2.61%, respectively.

Table 4 Summary of fuel properties of magnetite nano-particles with different concentrations

Base fuel	Nanoadditive proportions	Ultrasonication type/time/power	Fuel properties						Ref
			Viscosity (cSt)	Flashpoint (°C)	Fire point (°C)	Calorific value (KJ/kg)	Density (g/m3)	Cetane No.	
Rice Bran biodiesel	–	–	6.32	138		38123	0.882	52.0	[174]
	1%	sonication for 60 min	6.55	144	–	39143	0.910	55.0	
chicken fat methyl ester-CFB30	–	–	3.28	98	103	42228	0.850	49.5	[175]
	50 ppm	Titanium horn probe, 20 kHZ for 45 minutes	3.33	96	101	42503	0.851	51.4	
	100 ppm		3.37	94	99	42798	0.851	52.8	
	150 ppm		3.55	97	102	42720	0.856	54.1	
Waste cooking oil (B20)	–	–	3.29	85	88	39672	0.821		[176]
	25 ppm	Probe sonicator for 30 min	3.75	88	90	39546	0.824	–	
	50 ppm		4.34	89	92	39868	0.826	–	
	75 ppm		4.38	89	93	39868	0.829	–	
	100 ppm		4.42	85	88	40000	0.833	–	
Cauler-paRac-emosa Oil methyl ester(CROME)	–	–	6.30	138		38210	0.880	52.0	[53]
	1%	ultrasonic agitation for 60 min	6.55	144	–	39205	0.900	55.0	
Rice bran biodiesel	–	–	6.31	137		38223	0.881	52.0	[177]
	1.30%	–	6.56	143	–	39243	0.911	54.0	
Diesel		–		58		42000	0.815	47.0	[106]
	25 ppm	sonication for 30 min	–	63	–	42342	0.819	48.4	
	50 ppm		–	67	–	42657	0.823	49.6	
Pongamia biodiesel blends-B20	–	–	3.40	81		41600	0.859	51.4	[51]
	0.50%	–	3.47	81	–	41670	0.862	51.8	
	1.00%	–	3.55	81	–	41690	0.871	52.5	
	1.50%	–	3.63	81	–	41690	0.880	53.1	
Rice bran methyl ester	–	–	6.32	138		38123	0.882	52.0	[178]
	2%	–	6.55	144	–	39143	0.910	55.0	
Mahua oil methyl ester	–	–	5.97	136		37147		52.0	[109]
	1%	sonication for 60 min	5.45	143	–	38543	–	55.0	
chicken fat methyl ester-CFB10	–	–	2.81	80	85	42742	0.844	47.2	[103]
	50 ppm	50–60 kHz , and 1 kW for 10–40 min	2.85	78	82	43002	0.844	49.2	
	100 ppm		2.89	77	81	43319	0.845	50.5	
	150 ppm		2.95	78	82	43205	0.846	52.0	
chicken fat methyl ester-CFB20	–	–	3.05	89	94	42485	0.848	48.4	
	50 ppm	50–60 kHz , and 1 kW for 10–40 min	3.09	87	92	42761	0.848	50.3	
	100 ppm		3.13	85	90	43059	0.849	51.7	
	150 ppm		3.18	86	91	42980	0.849	53.4	
chicken fat methyl ester-CFB30	–	–	3.29	98	103	42228	0.851	49.5	
	50 ppm	50–60 kHz , and 1 kW for 10–40 min	3.33	94	101	42502	0.851	51.4	
	100 ppm		3.37	91	97	42798	0.852	52.8	
	150 ppm		3.54	93	98	42719	0.853	54.6	
Methyl Esters of Mustard Oil	–	–	6.22	140		38147	0.878	50.0	[179]
	1%	–	6.45	143	–	39227	0.922	54.0	
pongamia methyl ester-PME20	–	–	3.50	76	–	41580	0.843	49.0	[180]
	50 ppm	40 kHz and 120w for 60 minutes	3.70	48	–	42258	0.846	55.0	
	100 ppm		4.10	52	–	42631	0.848	56.0	

Table 4 (continued)

Base fuel	Nanoadditive proportions	Ultrasonication type/time/power	Fuel properties						Ref
			Viscosity (cSt)	Flashpoint (°C)	Fire point (°C)	Calorific value (KJ/kg)	Density (g/m3)	Cetane No.	
Diesel	–	–	3.50	58		42929	0.816	51.0	[104]
	30	40 kHz and 240 W for 40 min	3.60	63		43442	0.817	55.3	
	60		3.70	34		43657	0.821	55.9	
	90		3.80	67		43729	0.823	56.4	
chicken fat methyl ester-CFME20	–	–	3.05	89	94	42486	0.848	48.4	[87]
	50	Titanium horn probe and 20 kHz for 45 min	3.09	87	92	42762	0.848	50.3	
	100		3.13	85	90	43059	0.848	51.7	
	150		3.19	86	91	42980	0.849	53.4	

Venkata et al. [174] also examine the fuel properties by adding 1% of ferrofluid to rice bran oil. This increases kinematic viscosity by 3.56%, flash point by 3°C, water content by 0.02%, and other properties like density, calorific value, and cetane index are increased by 5.45%, 2.60%, and 2.97% individually. This is due to its huge surface area. Ferrofluid has highly significant catalytic activity, which prompts improvements in these characteristics. Karthikeyan et al. [53] found that the addition of ferrofluid changed all of the characteristics. When magnetite is added to the Caulerpa Racemosa Oil, methyl ester properties like density, flash point, kinematic viscosity, calorific value, and cetane index are improved, which also increases the water content by 0.02%. The water content increases somewhat since ferrofluid contain a significant amount of water.

Vinoothan et al. [176] have examined the improvement of fuel characteristics of B20 blend biodiesel from waste cooking oil with the concentrations of 25, 50, 75, and 100 ppm magnetite nanoparticles. The outcomes reveal that when the concentration of nanoadditive increases, fuel properties like calorific value, thickness, and viscosity are increased. According to the adding of magnetite nanoparticles to diesel raised the viscosity, calorific value, flash point, and cetane number. Dinesh et al. [109] investigated the addition of 1% magnetite to Mahua oil methyl ester and noticed a significant decrease in viscosity, as well as a rise in cetane number, calorific value, and water content by 0.05%. This is because of the presence of water in ferrofluid. The purpose of adding magnetite nanoparticles to diesel/biodiesel blends is to improve engine performance by increasing fuel characteristics such as density, flash point, calorific value, and cetane number.

Effect of magnetite nanoparticles on engine performance

Based on the findings of this study, several experiments show that adding magnetite nanoparticles to diesel or biodiesel fuel improves the thermo-physical properties [181–183], thereby increasing the calorific value and activating the atomization of droplets of the test fuel, which results in shorter ignition delay time and complete combustion [184]. Due to the ignition delay being shorter, more fuel is consumed in the pre-mixed combustion stage during the early-on part of the expansion stroke, resulting in less brake-specific fuel consumption (BSFC) [185]. Another aspect that may play a role is the high concentration of oxygen in additive mixes, which promotes better combustion and reduced fuel consumption [182–186].

Vinoothan et al. [176] noticed that the presence of magnetite nanoparticles in the fuel blend improves break thermal efficiency (BTE). At full load, the 100ppm B20 blend had the highest brake thermal efficiency (BTE) (i.e., 1.49% higher) and the lowest BSFC. Finally, it was concluded that 100ppm magnetite nanoparticles in the B20 blend of waste cooking oil methyl ester is the optimum blend for improving CI engine performance. Shafii et al. [102] examined the impacts of 0.4 and 0.8% concentrations of water-based ferrofluid on diesel fuel in a 2200 rpm operated 4-stroke diesel engine. According to the findings, 0.4% ferrofluid lowers the BSFC by 3.23–6.45% while increasing it by 3.33–6.89%, BTE, whereas 0.8% ferrofluid lowers the BSFC by 5.06–10.85% while increasing it by 5.33–12.17%. Yuvarajan et al. [121] investigate the effects of adding magnetite to rice bran oil methyl esters in a constant speed diesel engine. From the results, it was shown that performance was improved by 4.27% and decreased by 5.17% BSFC. This is due to increased oxygen accessibility, which improves air-fuel mixing during combustion. Ferro fluid additionally has positive combustion properties, such as high temperatures of combustion and rapid energy release rates. Sayed et al. [106] use an air-cooled four-stroke diesel engine with a 300 bar injection pressure. The outcomes reveal that the 25ppm nanoblended fuel gives almost the same BSFC as diesel fuel, while 50 ppm fuel shows a significant decline of roughly 9% when compared to different samples. But in the case of brake thermal efficiency, 50ppm gives around 2% increment. This is because of the nanoparticles' large surface area and significant chemical reactivity, which lead to an improvement in the ignition effectiveness of the nanoparticle blended diesel fuel.

Shiva Kumar et al. [51] have examined the B20 blend of pongamia methyl ester with ferrofluid with different proportions. From the outcomes, it was shown that a higher value of BSFC and a lower value of BTE were found for biodiesel-diesel blend when compared with diesel due to viscosity and lower calorific value. When adding ferrofluid to the B20 blend, there is an improvement in performance, and the blend with 1% additive gives the least BSFC and maximum BTE. Dinesh et al. [109] used 14-nm size magnetite nanoparticles in Mahua Oil Methyl Ester, which showed an increase in BTE of about 5.27% and a decrease in BSFC of about 5.37%. This is due to the fact that nanosized ferro-additives have a shorter igniting delay [180]. Sarath et al. [187] examined the impacts of 4%, 8%, and 12% ferrofluid on diesel and showed that there were decreases in BSFC by 6.06–9.09%, 8.00–15.15%, and 10.52–18.18%. Similarly, BTE rises by 6.21–9.10%, 9.6–16.69%, and 11.07–21.43%, respectively. Based on the observations, it was concluded that ferrofluid added to diesel fuel has a significant effect on performance. Ranaware et al. [188] examined the cerium oxide and ferrofluid nanoadditives to the diesel on a 4 stroke DI variable compression ratio engine as an experiment. From the results, it was shown that ferrofluid added to diesel fuel increases up to 12% BTE and decreases up to 11% BSFC relative to diesel fuel. Ameer et al. [175] explore the impacts of magnetite nanoparticles in chicken fat biodiesel blend with hydrogen induction on the DICI engine. From the investigational results, 30% chicken fat biodiesel blend (CFB30) blend added magnetite nanoparticle shows a 7.49% improvement in BTE and a 22.86% decrease in BSFC compared with the CFB30 blend. When hydrogen injection of 10 lpm was introduced, there was a 5.08% increase in BTE and a 14.17% decrease in BSFC. Table 5 summarizes the engine performance with various concentrations of magnetite nanoparticles in the diesel/biodiesel blend.

Effect of magnetite nanoparticles on engine combustion characteristics

Cylinder pressure

Combustion characteristics are important features that reflect the engine's combustion efficiency and have a significant impact on engine performance and emissions. To evaluate this, two key parameters are typically used, i.e., heat release rate (HRR) and pressure rise rate (PRR). Figure 9 illustrates the effect of nano-added diesel or biodiesel on the timing of P_{max} inside the combustion chamber. Figure 9A [106] shows that the pressure starts increasing significantly from 7° before TDC for 50ppm nanoblended diesel and has a peak pressure of 73.70 bars. This is due to the high surface areas of nanoparticles, which increase their chemical reactivity, which in turn reduces the ignition delay. Figure 9B [191] shows the impact of Al_2O_3 and Fe_3O_4 nanoparticles on in-cylinder pressure, in which both the nanoblends have increased cylinder pressure compared with the biodiesel blend. Figure 9C [180] shows the variation of cylinder gas pressure when the engine was fueled with 20% pongamia methyl ester with 50,100 ppm nanoparticles and shows that the iron oxide nanoparticles added blends have a higher peak pressure. Figure 9D [109] shows the pressure variation when nanoblends with surfactant are used. It shows that the lower peak pressure of the nanoblend is due to the viscosity of the nanoblend being higher, causing atomization and mixing of fuel with air to be uneven, resulting in longer breakup length, lower dispersion rate, and increased ignition delay. Figure 9E, F [100] shows that pressure increases significantly from 7° before TDC for 40 ppm iron oxide nanoblend and 8° before TDC for 40 ppm aluminium oxide nanoblend fuel. Further, there are no major changes in the dosage level of nanoparticles. Figure 9G, H [104] examines the rate of pressure rise at 1800 rpm under 50% and full engine load, revealing increases of 0.7%, 1.2%, and 3.1% at 50% engine load, and 1.7%, 2.8%, and 3.6% at full load for diesel+ 30ppm Al_2O_3 + Fe_2O_3 nanoblend, 90ppm Al_2O_3 blend, and finally, 90ppm Fe.

Heat release rate

Figure 10 depicts the fluctuation of heat release rate with crank angle of different nanoparticle doses. The heat release rate was found to be typically enhanced with the inclusion of nanoparticles, as shown in Fig. 10A [106] According to the author's findings, the greatest amount of heat released rate for 50 ppm nanoblend was 168.468 kJ/m^{3}c owing to the fuel's faster combustion and shorter ignition latency. The degree of fuel-air mixing and uniform burning may have improved as a result of a shorter ignition delay. The addition of Al_2O_3 and Fe_3O_4 nanoparticles to biodiesel increased the rate of heat release, as shown in Fig. 10B [191]. From the author's finding, the maximum amount of heat release rate for 80ppm Fe_3O_4 nanoblend is 114.82 kJ/m^{3}c and for 120ppm there is a slight decrease, but when compared with the biodiesel blend, the HRR for all the nanoblends is increased. Figure 10C [180] shows the variation of HRR when the engine was fueled with 50,100 ppm of 20% pongamia methyl ester, which shows that the heat release rate was observed for iron oxide nanoparticles added blends. Figure 10D, E [100] depicts the 20% biodiesel blend with 40ppm and 80ppm nanoparticles, which shows that the HRR is 124.747, 132.828, and 137.938 kJ/m^{3}c for the 20% biodiesel blend, 40ppm Fe_2O_3 blend, and 40ppm Al_2O_3 blend, and finally, it was stated that increasing the nanoparticle dosage level tends to enhance the heat release rate. Figure 10F [109] depicts the change in HRR

Table 5 Summary of magnetite nanoparticles on engine performance with various concentrations

Base Fuel	Nano particles concentration	Surfactant	Engine	Engine Performance		Ref
				BTE	BSFC	
Waste cooking oil	25,50,75 & 100 ppm	—	4 strokes, 1- cylinder, VC ratio CI engine	Increases by 1.49%	Decreases by 2.21%	[176]
Diesel	0.4% , 0.8%	—	4-cylinder, 4-stroke, CI engine, water cooled 43kW at 4800 rpm	Increasing up to 12%	Decreasing up to 11%	[102]
Diesel	0.4% , 0.8%	—	1-cylinder, 4-stroke, water-cooled, 9 hp,2200 rpm	—	No significant variation	[189]
Rice bran oil	1.30%	0.2 % tri methyl ammonium hydroxide	1-cylinder 4-stroke diesel engine 4.45 kW @ 1500 rpm	Increases by 4.27%	Reduced by 5.17%	[177]
Diesel	25 and 50 ppm	—	4-stroke, 1- cylinder, air cooled 5.2 kW at 1500 rpm.	Increases by about 2%	Decreases of about 9%	[106]
Mahua oil	40, 80 ppm	—	4-stroke, 1 cylinder diesel engine, 3.7 kW at 1500 rpm	Increases	Decreases	[100]
pongamia oil	0.5%, 1% % 1.5%	—	4- stroke 1- cylinder, water cooled CI engine, 1500 rpm	Increase up to 16.6 %	Decreases by 8%	[51]
Mahua oil	1%	0.3 % tri methyl ammonium hydroxide	2- cylinder, 4- stroke, air cooled diesel engine, 1300 rpm	Increases of about 5.27%	Decreases of about 5.37%.	[109]
diesel	0.4% , 0.8%	—	four stroke diesel engine	Increases up to 12%	Decreases up to 11%	[190]
diesel	4%, 8%, 12%	—	4 stroke 1- cylinder, water cooled CI engine, 5 Hp,1500 rpm	Increased by 11.07 – 21.43 %.	Decreases up to 10.52 – 18.18%	[187]
diesel	0.4%, 0.8%	tetra-methyl-ammonium hydroxide	1-cylinder 4-stroke direct injection VC ratio engine.	Increases up to 12%	decreases up to 11%	[188]
Mahua oil	40, 80 & 120 ppm	cetyltrimethyl ammonium bromide	4-stroke, 1-cylinder, common rail direct injection, water cooled, 1500 rpm, 3.7 kW	Increased up to 0.44%,	—	[191]
chicken fat oil	50, 100 and 150 ppm	—	4-stroke, 1-cylinder, DI engine, water-cooled CI engine, 3.5 kW @ 1500 rpm	Increases by 7.49%	Reduction by 22.86	[175]

Table 5 (continued)

Base Fuel	Nano particles concentration	Surfactant	Engine	Engine Performance		Ref
				BTE	BSFC	
chicken fat oil	50, 100 and 150 ppm	—	1-cylinder, 4-stroke, dual DI engine, water-cooled CI engine, 3.5 kW @ 1500 rpm	Improved by 4.84%,	Reduction by 10.44%	[87]
Mustard Oil	0.01	0.3%of surfactant	4 stroke, 1 cylinder diesel engine, 4.4 kW at 1500 rpm	Increases by 5.122%	Decrease by 4.72%	[179]

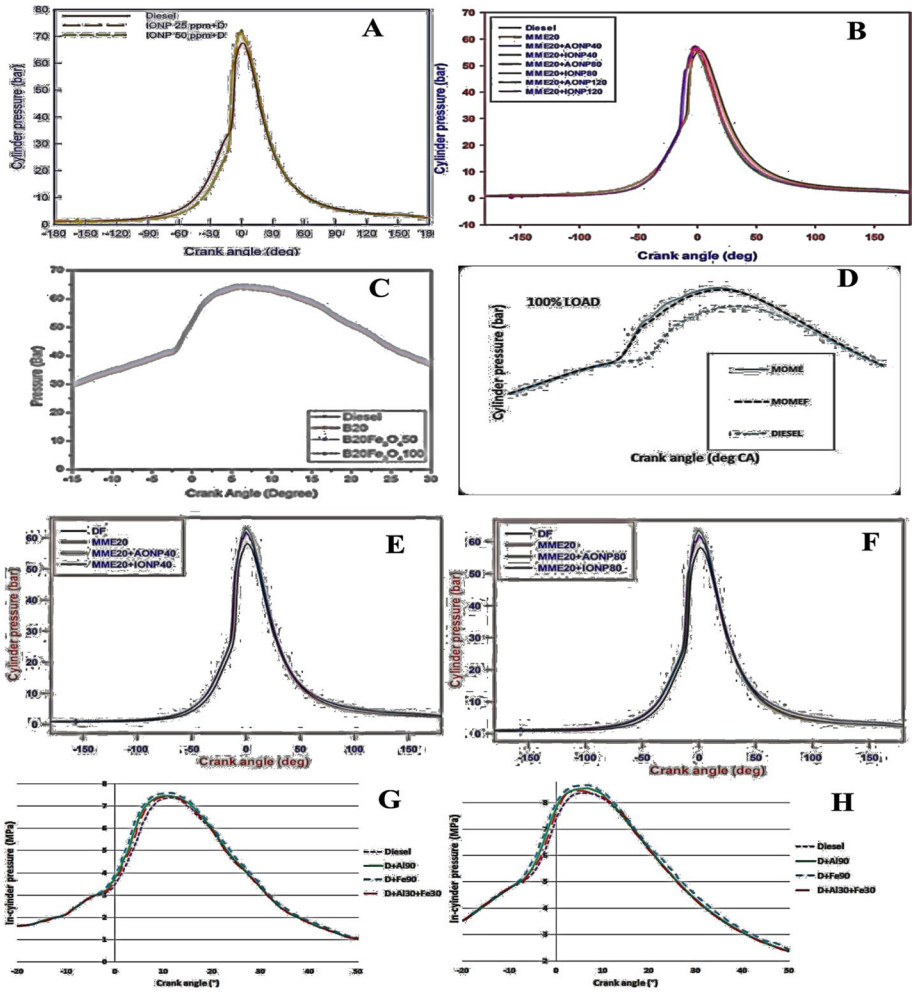

Fig. 9 Effect of cylinder pressure on nano-added diesel or biodiesel

when the engine was driven with nanoblends containing surfactant. From the author's finding, the maximum HRR of diesel, nanoblend, and MOME is 76.44, 70.66, and 66.80 J/°CA, respectively. Due to the longer delay period, the peak heat release rate occurs in

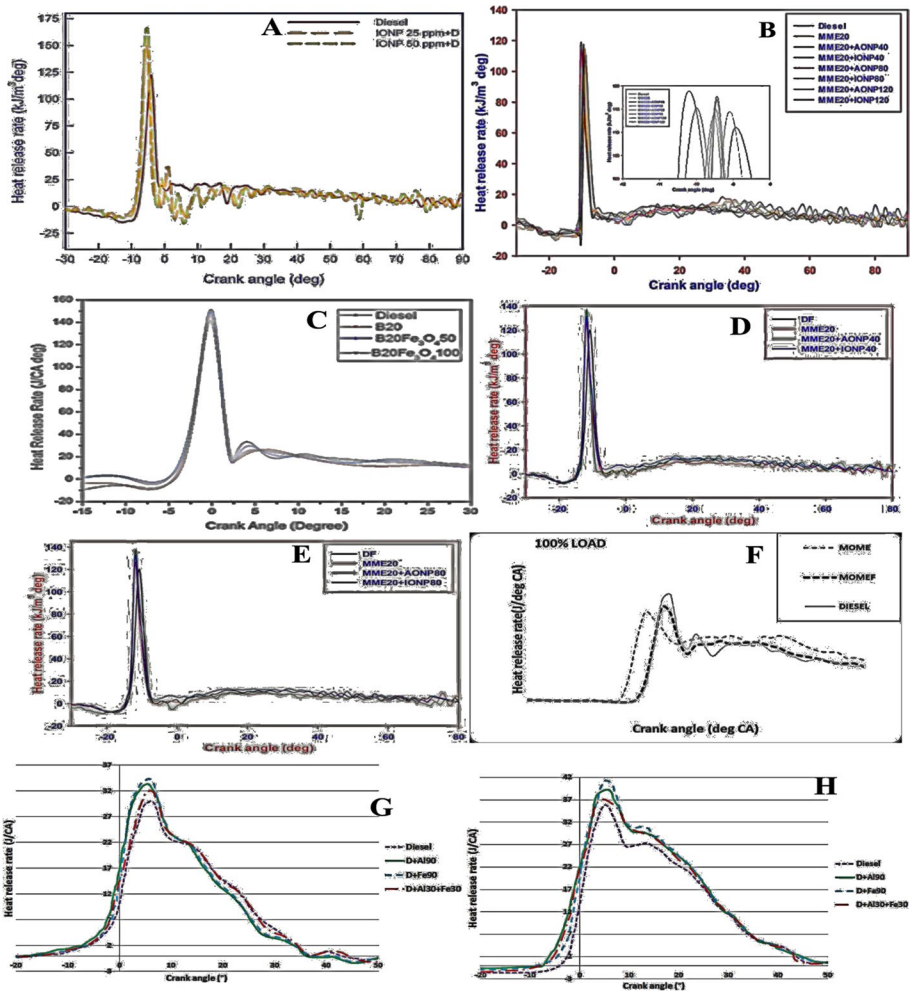

Fig. 10 Effect of heat release rate on nano-added diesel or biodiesel

the latter part for MOME and nanoblend in comparison to diesel. Figure 10G, H [104] shows the maximum heat release rate of the engine increased by 3.4%, 9.4%, and 15.2% at full load. Furthermore, the maximum HRR for 50% load was 6.8%, 11%, and 13.9% for diesel+, 30ppm $Al_2O_3 + Fe_2O_3$ nanoblend, 90ppm Al_2O_3 blend, and 90ppm Fe_2O_3 blend.

Ignition delay

The time duration between the initiation of fuel injection and the beginning of combustion is referred to as the ignition delay period. Figure 11A [128] illustrates the addition of alumina nanoparticles to diesel, which was found to reduce ignition delay due to improved combustion of the air-fuel combination by increasing the surface area to volume ratio. Dose concentrations of 20, 30, and 40ppm of Al_2O_3 nanoparticles added to diesel fuel resulted in 11%, 25%, and 37% reductions in ignition delay, compared to crude diesel at full load. Figure 11B, C [192] shows a 5.47% and 0.99% reduction in delay duration for TiO_2 and Al_2O_3 added diesel of 25 ppm at full load, respectively. As seen

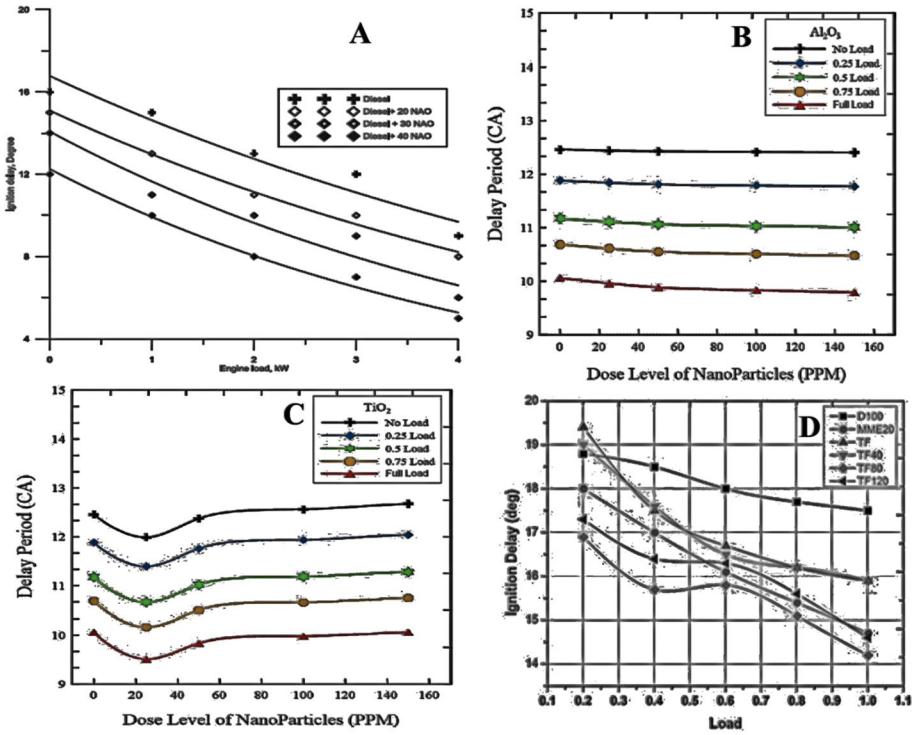

Fig. 11 Effect of Ignition delay of nano-added diesel or biodiesel

in Fig. 11D [193], the addition of iron oxide nanoparticles to the ternary fuel reduced the delay period as compared to pure diesel. The shorter delay period is attributable to improved atomization due to the high surface tension and calorific value of the blend. Furthermore, the existence of iron oxide nanoparticles and pentanol, both of which tend to raise the latent heat of fuel blends, impedes the synthesis of carbon chain molecules.

Cylinder temperature

Figure 12A [128] illustrates the effect of aluminium nanoadditive in pure diesel on cylinder temperatures, indicating that adding Al_2O_3 additives to diesel fuel reduces ignition delay, increases peak cylinder pressure, and also improves HRR, which results in a rise in cylinder temperature. Peak cylinder temperatures at full load for diesel, 20, 30, and 40 ppm nanoadditives are 1470, 1510, 1570, and 1620K, respectively. Figure 12B [194] depicts the waste cooking oil biodiesel with TiO_2 nanoadditive and shows the mean cylinder temperatures were to be 1270, 1000, 1030, 1080, and 1160 K for diesel, B20, 25ppm, 50ppm, and 100ppm of nanoblends, respectively. The aluminium nanoadditive in 20% calophyllum inophyllum biodiesel enhances the mean cylinder gas temperature, as seen in Fig. 12C [195]. Peak mean cylinder gas temperatures at full load are 1475, 1457, 1496, 1405, and 1416°C for diesel, 20% CIB, 40ppm, 20% CIB+ 20% EGR, and 40ppm+20% CIB + 20% EGR fuel samples, respectively. Figure 12D [196] depicts the change of in-cylinder temperature on a CRDI engine. According to the graph, the mean cylinder temperature of all nanofuel blends at dose rates of 30, 60, and 120 mg/L revealed a rise in the temperature of the cylinder.

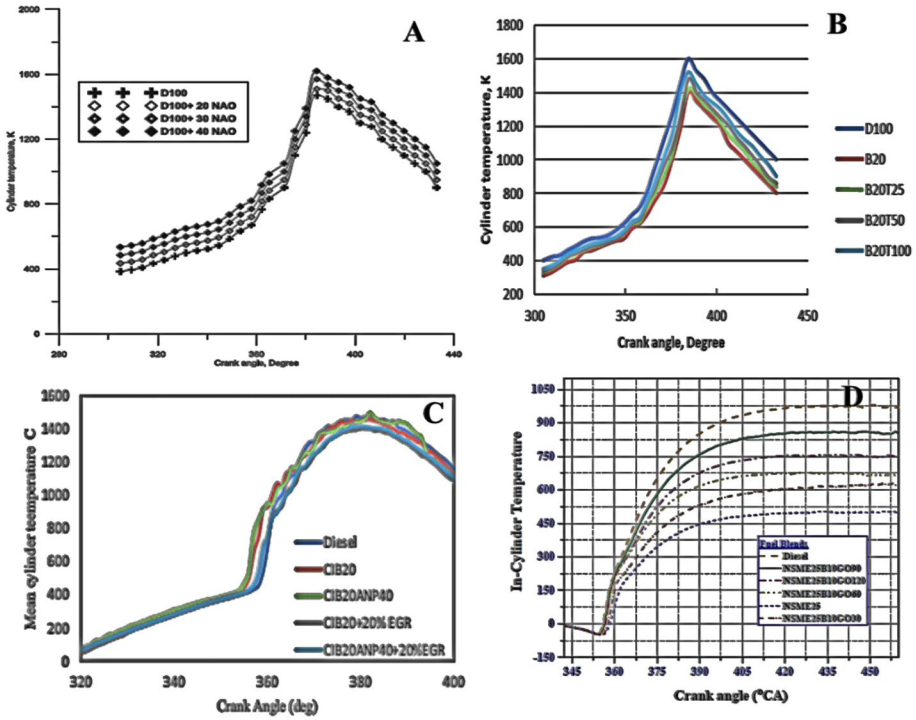

Fig. 12 Effect of cylinder temperature of nano-added diesel or biodiesel

Combustion duration

The presence of nanoparticles causes a micro-explosion of the fuel droplets, which accelerates fuel air mixing and evaporation, which shortens the length of the combustion. Figure 13A [197] illustrates the variance in combustion duration for a 20% honge oil methyl ester blend with aluminium oxide nanoparticle concentrations of 20, 40, and 60 ppm found to be 30°CA, 27°CA, and 29°CA, and 47°CA, 42.8°CA, and 45°CA, respectively, under zero and full load conditions. The combustion duration with nanoparticles in diesel at various engine loads is depicted in Fig. 13B [128]. According to the graph, the combustion time values at full load are 74°CA, 70°CA, 66°CA, and 61°CA for diesel, and 20, 30, and 40 ppm for nanoblends. At 100% load, Fig. 13C [198] shows a 20% microalgae blend with 0.1 and 0.2% (vol./vol.) Al_2O_3 nanofluid, with combustion durations of 67° CA, 58° CA, and 47° CA, respectively. According to the graph, the Al_2O_3 nanoblend has a shorter combustion time than the 20% microalgae blend. This is due to the Al_2O_3 nanoblend's decreased density and viscosity, which causes the improved combustion. Figure 13D [199] illustrates the combustion duration of each fuel under various operating conditions. According to the graph, at high speeds, the combustion duration of fuel is somewhat shorter than that at low speeds since the mixing speed of fuel and air is quicker, and therefore, the combustion speed rises. The burning time of the 100ppm nanoblend fell by 6.74% and 7.30% rpm at 1000 and 1800 rotational speeds, respectively.

Effect of magnetite nanoparticles on emission characteristics

The major challenge of the twentyfirst century is likely to be global climate change, and it has risen to 1.4–5.8°C by the year 2100. Pollutants like carbon dioxide (CO_2), water

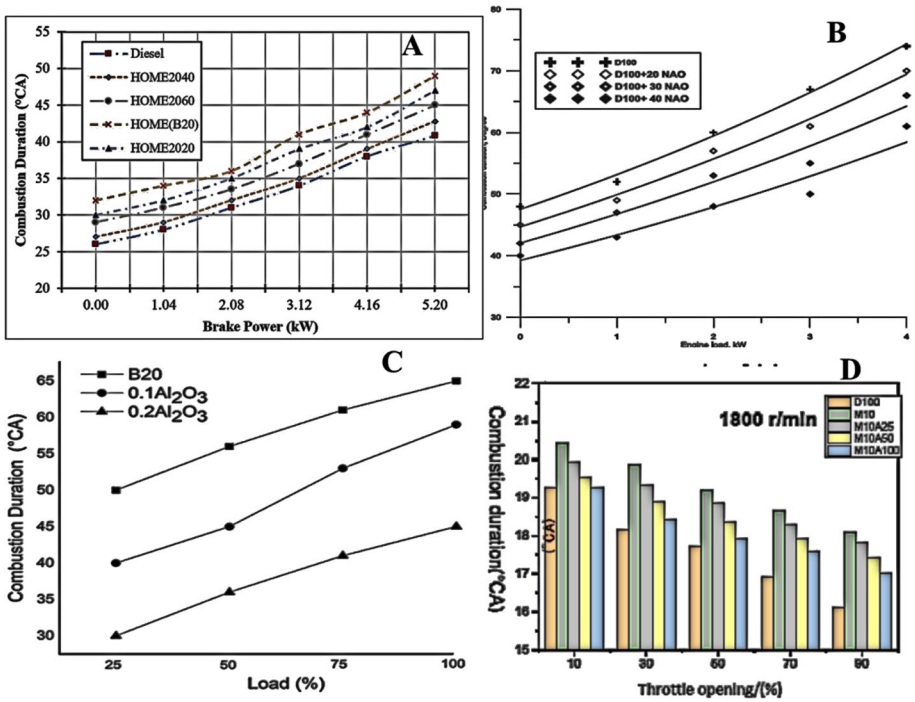

Fig. 13 Effect of combustion duration of nano-added diesel or biodiesel

vapor, methane (CH_4), sulphur dioxide (SO_2), and nitrogen dioxide (NO_X) are the major contributors to climate change. Researchers have concentrated on creating a wide range of renewable energy sources to minimize these emissions into the environment, including oxygenated fuels, biofuels, fuel cells, and solar technologies. Because of their strong thermal braking performance, high compression ratio, and reduced air-fuel mix, the use of fossil fuel in diesel engines has an outstanding reputation for low fuel consumption, high dependability, and high durability. However, both diesel and biodiesel fuels have their respective limitations in producing higher NO_X, which leads to poor combustion performance. Thus, to overcome these limitations, the addition of fuel additives like magnetite nanoparticles is gaining much attention to improve the oxidation characteristics of biodiesel since magnetite nanoparticles have an excess of oxygen that promotes better combustion and lower fuel usage. This section provided a critical review of the most recent research papers on the effect of nanofuel additives on diesel engine emissions. Table 6 summarized the influences of magnetite nanoparticles in various fuel blends on emission characteristics with various concentrations.

Karthikeyan et al. [53] explored the impacts of ferrofluid mixed with Caulerpa racemosa oil methyl ester as a test fuel. The base fuel is treated with 1% ferrofluid and 0.3% surfactant $(CH_3)_3NOH$). It was revealed from the test that harmful pollutants such as HC, CO, NO_X, SO_2, and smoke were drastically reduced when compared to diesel. Venkata et al. [174] investigated a four-stroke single chamber, air-cooled diesel engine with magnetite nano-added rice bran oil methyl ester blend. From the experimentation, there is a decrease of 19 ppm, 0.011%, and 93 ppm in HC, CO, and NO_X, and also 9% of smoke opacity is decreased. Yuvarajan et al. [178] have also examined the rice bran oil methyl ester with magnetite nano in a two-chamber CI engine. From their outcomes,

Table 6 Summary of magnetite nanoparticles on Emission characteristics with various concentrations

Base Fuel	Dosage	Surfactant	Engine	Emissions				Ref
				HC	CO	NO_X	Smoke	
CaulerpaR-acemosa Oil	1%	0.3 % tri methyl ammonium hydroxide	1-cylinder 4-stroke diesel engine @ 1500 rpm, 5.2 kW	Decreases	Decreases	Decreases	Decreases	[53]
Rice bran oil	1%	0.3% tetra methyl ammonium hydroxide	1-cylinder 4-stroke diesel engine 4.45 kW @ 1500 rpm	Decrease by 19ppm	Decrease by 0.011%	Decrease by 93ppm	Decrease by 9%	[174]
Rice bran oil	2%	0.3% tri methyl ammonium hydroxide	2-cylinder,4-stroke diesel engine @ 1500 rpm	Decreases by 10.8%	Decreases by 9.1%	Decreases by 8.49%	Decreases by 3.85%	[178]
Diesel	0.4% , 0.8%	—	1-cylinder, naturally aspirated, 4-stroke, water-cooled, 9 hp,2200 rpm	—	Increases	Average reductions of around 56% and 67%	Increases	[189]
waste cooking oil	25,50,75 & 100 ppm	—	4 strokes, 1- cylinder, VC ratio CI engine	—	Decreases by 2.08%,	Decreases by 7.43%,	Decreases by 10.43%	[176]
Diesel	0.4% , 0.8%	—	4-cylinder, 4-stroke, CI Engine @ 4800 rpm, 43kW	—	Increases	Decreases	—	[102]
Rice bran oil	1.30%	0.2 % tri methyl ammonium hydroxide	1-cylinder 4-stroke diesel engine 4.45 kW @ 1500 rpm	Reduced by 10.8%	Reduced by 9.1%	Reduced by 8.49%	—	[177]
Diesel	25 and 50 ppm	—	4 strokes, 1-cylinder, air cooled 5.2 kW at 1500 rpm.	Decreases	Decrements are about 48% and 52%	Increases	Decreases	[106]
Mahua oil	40, 80 ppm	—	4stroke, 1 cylinder diesel engine, 3.7 kW at 1500 rpm	Decreases	Reduced about 18%	Increases	Decreases by about 15-18%,	[100]
Pongamia oil	0.5%, 1% % 1.5%	—	4 stroke 1- cylinder, water cooled CI engine, 1500 rpm	Decrease to 22.9%	Reduced to 35.8%	Decreases	Decrease to 24.4 %	[51]
Mahua oil	1%	0.3 % tri methyl ammonium hydroxide	4- stroke,2-cylinder, diesel engine @ 1300 rpm	Reduced by 10.8%,	Reduced by 6.44%	Reduced by 9.49%,	Average of 14.28% reduction	[109]
diesel	0.4% , 0.8%	—	four stroke diesel engine	Reduced by 6.39%	Reduced by 10.24%	Decreases	Reduced by 5.38%	[190]

Table 6 (continued)

Base Fuel	Dosage	Surfactant	Engine	Emissions				Ref
				HC	CO	NO_x	Smoke	
diesel	4%, 8%, 12%	—	4 stroke 1- cylinder, water cooled CI engine, 5 Hp,1500 rpm	—	Increased by 30-43 ppm	Decreased by 17 -30 ppm	—	[136]
diesel	0.4%, 0.8%	tetra-methyl-ammonium hydroxide	1-cylinder 4-stroke direct injection VC ratio engine.	—	Increased by 21 to 42 ppm.	Decreased by 14 to 24ppm.	—	[187]
Mahua oil	40, 80 & 120 ppm	Cetyltri-methyl ammonium bromide	4-stroke, 1-cylinder, common rail direct injection, 1500 rpm, 3.7 kW	Decreases	Reduced up to 11.32%	Slightly increases	Decreases up to 15–18%,	[191]
chicken fat oil	50, 100 and 150 ppm	—	4-stroke, 1-cylinder, DICI engine @ 1500 rpm, 3.5 kW	Decreases by 22.27%,	Decreases by 0.119%	Decreases by 15.72%,	Decreases by 15.64%	[175]
chicken fat oil	50, 100 and 150 ppm	—	4-stroke, 1-cylinder, DICI engine @ 1500 rpm, 3.5 kW	Reduction by 21.73%	Reduction by 53.22%,	Reduction by 15.39%	Reduction by 14.73%	[87]
Mustard oil	1%	0.3%of surfactant	4 stroke, 1 cylinder diesel engine, 4.4 kW at 1500 rpm	Reduction by 5.8%	Reduction by 2.66%	Reduction by 7.74%	Reduction by 6.98%	[179]
Pongamia oil	50, 100 ppm	—	4 stroke, 1 cylinder diesel engine, 3.7 kW at 1500 rpm	Decreases	Decreases	Slightly increases	Decreases	[180]

an improvement of 6.34%, 6.34%, 8.49%, and 3.85% in CO, HC, NO_X, and smoke was obtained. Syed et al. [106] utilize the mechanical homogenizer and an ultrasonicator for the mixing of 25 and 50 ppm of iron oxide nanoparticles, respectively. From the outcomes, the nano-mixed diesel shows a 52% decrease in both HC and CO, and there is a marginal increment in NO_X emissions. Also, it was noticed that 50 ppm of nanoblended fuel gives the optimum dosing level. Vinoothan et al. [176] inspected the magnetite nanofluid with 20% waste cooking oil at 200 bar injection pressure, 17.5 compression ratio with varying the load. From the outcomes, at full load for 100 ppm bended B20 fuel, the NO_X, CO, and smoke all show decreases of 7.43%, 2.08%, and 10.43%. Shafii et al. [102] performed a test with 0.4 and 0.8% ferrofluid in a four-stroke diesel engine operating at 2200 rpm. It was shown that ferrofluid added to diesel blend improves engine performance as well as decreases NO_X emissions, but there is an increment in CO outflows. Nasrin et al. [189] investigated the capability of Fe_2O_3 nanoparticles as an additive in fuel at 0.4 and 0.8% volumetric fractions in a direct-infusion diesel engine. From the review, 0.8% nanoblend shows better combustion characteristics when compared with

0.4% nanoblend fuel. The exhaust emissions like NO_X and SO_2 outflows decrease drastically, while there is an increase in CO and smoke opacity was noticed with the increased nanoparticle dosing levels. Finally, it was noticed that the proper selection of nanoparticle dosing level should be considered. Aalam et al. [100] investigated the effects of a 20% Mahua methyl ester (MME20) blend with aluminium oxide and iron oxide nanoparticles at different concentrations (40 ppm and 80 ppm) on a CRDI single-cylinder diesel engine. The outcomes show that the degree of harmful contamination like HC, CO, and smoke was essentially decreased when compared with the MME20 blend and neat diesel.

Kumar et al. [51] have utilized the B20 blend of pongamia biodiesel with ferrofluid on a Kirloskar TV1 engine at various loads, keeping 1500 rpm as a steady speed. When the ferrofluid was added to the blend, CO and HC decreased by 35.8% and 22.9%, respectively, at full load. At last, it was concluded that the 1% ferrofluid of the B20 blend gives maximum efficiency and fewer emissions compared to all the other blends. Sarath et al. [187] explored the impacts of 4%, 8%, and 12% ferrofluid in diesel fuel at an engine speed of 15,000 rpm. From the outcomes, it was shown that emissions like nitrogen oxides and particulate matter have a decreasing trend while other emissions such as HC and CO show an increasing trend when the concentration of ferrofluid content of the blend increases. Ranaware et al. [188] have shown the impact of utilizing various nanoadditives like cerium oxide and ferrofluid in diesel fuel. From the observations, it was shown that adding 0.4 and 0.8 water-based ferrofluid to diesel fuel not only reduces NO_X emissions but also slightly increases CO emissions. Syed [191] changed the dosing amount, i.e., from 40 to 120 ppm nanoparticles in a MME20 fuel blend. The results show that 80 ppm of both nanoadditives gives the best emission characteristics. Similarly, an 80 ppm Al_2O_3 nanoblend shows better combustion characteristics when compared with magnetite nanoparticles. Ameer et al. [175] researched the impacts of magnetite nanoparticles in chicken fat biodiesel blend, i.e., CFB30, and also hydrogen induction on a DICI engine. From the outcomes, it was shown that for 100ppm nanoblend the decrease in NO_X, smoke, UHC, and CO was by 15.72%, 15.64%, 22.27%, and 0.119, respectively, relating to the CFB30 blend. Similarly, injecting 10 lpm of hydrogen into the fuel causes the outflows like smoke, UHC, and CO to decrease by 11.57%, 14.7%, and 0.037 (vol.), while slightly increasing NO_X emissions. Based on the findings, it is determined that CFB30 nanoblend fuel combined with 10 lpm hydrogen enhances direct injection compression ignition (DICI) engine performance overall.

Conclusions

This review covers a brief overview of magnetite nanoparticle-based additives with a focus on the synthesis of nanoparticles, preparation and stability of nanofuels, and application of magnetite nanoblends in the diesel engine were analyzed thoroughly.

- The two chemical synthesis methods have been shown to be straightforward and cost-effective. The co-precipitation method by ultrasonic waves and magnetic field-assisted has shown excellent properties, and the effect of their binary combination on CCP synthesis was investigated and optimized for large-scale preparation of mag-

netite nanoparticles. The sol–gel method with varying annealing temperatures indicated that the different sized nanoparticles were obtained.

- ➢ Different techniques such as sedimentation, zeta potential testing, UV–Vis spectrophotometer, and turbidity meter are used to study the stability of nanofluids.
- ➢ Adding magnetite nanoparticles to diesel and biodiesel causes them to increase the calorific value and cetane number, improving combustion characteristics such as ignition delay time, heat release rate, and rate of pressure rise. The other properties like density, kinematic viscosity, and flash point are improved.
- ➢ The incorporation of magnetite nanoparticles into biodiesel or diesel allows for the release of high heat and a faster rate of energy release during the combustion process. As a result, there was an increase in BTE and braking power, but BSFC tended to decrease.
- ➢ The addition of magnetite nanoparticles to biodiesel/diesel reduces CO, HC, NO_X emissions, and smoke opacity significantly. These favorable results were achieved as a result of the high oxygen concentration and catalytic oxidation.

Challenges and future directions

Challenges

Magnetite nanoparticles are increasingly being used in IC engines to improve efficiency, combustion, and pollution. However, there are several problems and obstacles associated with using nanoparticles in real-world applications. As a result, new study possibilities for scientific writers and researchers all around the world have emerged.

- ➢ Even though the synthesis of magnetite nanoparticles is less costly than traditional techniques and is highly recommended for large-scale production, an adequate selection of mechanisms, process parameters, and equipment is required for the entire process to be completed, which adds to the overall cost. As a result, the high cost may limit its potential industrial applicability.
- ➢ The dispersion nanoparticles, which create a clogging effect mostly owing to agglomeration, have a substantial impact on the stability and thermo-physical characteristics of nanofluids. As a result, uniform dispersion of nanoparticles into the base fluid is a key step in creating excellent, homogeneous, and stable nanofluids. Instability can be reduced by using proper preparation procedures and enhancing mechanisms.
- ➢ The widespread and increased use of nanoparticles not only improves performance but also raises safety and health issues due to their discharge from exhaust gases. Due to their small size, they may readily enter biological systems and cause harm to the lungs, brain, and other internal organs. As a result, trapping nanoparticles from exhaust gas is highly recommended. Magnetite nanoparticles demonstrated minimal toxicity and the ability to be gathered by a magnetic bar, making them acceptable diesel fuel modifiers.

Future directions

Future studies on magnetite nanoparticle synthesis will add to the body of knowledge about the different parameters that influence the synthesis process and advanced

characterization approaches for effective future applications. As a result, adopting both cost-effective and environmentally friendly approaches is always critical in avoiding difficulties such as expensive materials, instrument rust, health concerns, and environmental pollution. Furthermore, enhancing the stability and thermal properties of nanofluids would lessen the challenges associated with their utilization in practical applications. The following are some of the prospective directions for magnetite nanoblend research:

- The stability of magnetite nanoblends is a major challenge that needs to be further investigated, mainly considering the effects of nanoparticle nature and morphology, ultra-sonication time, particle-particle interaction, base fluid-particle interaction, temperature, and time.
- Investigations into the thermophysical properties of nanoblends are to be continued as they are largely affected by the dispersed nanoparticles in base fluids, which provide a clogging effect mainly due to agglomeration.
- Additional research is required on the performance and emission characteristics of test fuels under various operating situations, such as injection timing, engine speed, and compression ratio.

Abbreviations

MRFR	Marker Research Future Reports
SEM	Scanning electron microscopy
XRD	X-ray diffraction
TEM	Transmission electron microscopy
PVP	Polyvinyl pyrrolidone
NTU	Nephelo turbidity unit
CFME	Chicken fat methyl ester
CFB30	30% Chicken fat biodiesel blend
CROME	Caulerpa racemosa oil methyl ester
MOME	Mahua oil methyl ester
MME20	20% Mahua methyl ester
CNT	Carbon nanotubes
DICI	Direct injection compression ignition
CRDI	Common-rail diesel engine
BSFC	Brake-specific fuel consumption
BTE	Brake thermal efficiency
UHC	Unburned hydrocarbons
TEOS	Tetra-ethyl ortho silicate
MWCNT	Multi-walled carbon nanotubes
GNP	Graphene nanoplatelets
CI	Compression-ignition
ppm	Parts per million
UV-Vis	Ultraviolet-visible spectrophotometry
HC	Hydrocarbons
CO	Carbon monoxide
rpm	Revolutions per minute
kW	Kilowatt
ANCF	Al_2O_3-Nb_2O_5/CeO_2/Fe_2O_3
HRR	Heat release rate
PRR	Pressure rise rate
TDC	Top dead center
CIB	Calophyllum inophyllum biodiesel
EGR	Exhaust gas recirculation

Acknowledgements
Not applicable.

Authors' contributions
The research reported in this paper was conceptualized by MSR. The methodology was suggested by CHSR and ASK. The manuscript was prepared by MSR, CHSR, and ASK supervised the research. The authors read and approved the final manuscript.

Funding
The authors received no financial support for the research, authorship, and publication of this article.

Availability of data and materials
Not applicable.

Declarations

Ethics approval and consent to participate
Not applicable.

Consent for publication
All the authors have consented for publication of the manuscript.

Competing interests
The authors declare that they have no competing of interests.

Received: 16 April 2022 Accepted: 25 July 2022
Published online: 05 September 2022

References

1. Kadarohman A, Hernani FK, Astuti RM (2010) A potential study on clove oil, eugenol and eugenyl acetate as diesel fuel bio-additives and their performance on one cylinder engine. Transport 25(1):66–76. https://doi.org/10.3846/transport.2010.09
2. El-Seesy AI, Hassan H, Ookawara S (2018) Effects of graphene nanoplatelet addition to jatropha biodiesel–diesel mixture on the performance and emission characteristics of a diesel engine. Energy 147:1129–1152. https://doi.org/10.1016/j.energy.2018.01.108
3. Aalam CS, Saravanan CG (2017) Effects of nano metal oxide blended Mahua biodiesel on CRDI diesel engine. Ain Shams Eng. J. 8(4):689–696. https://doi.org/10.1016/j.asej.2015.09.013
4. Sadhik Basha J (2018) Impact of carbon nanotubes and di-ethyl ether as additives with biodiesel emulsion fuels in a diesel engine – an experimental investigation. J. Energy Inst. 91(2):289–303. https://doi.org/10.1016/j.joei.2016.11.006
5. Bazooyar B, Hosseini SY, Begloo SMG, Shariati A, Hashemabadi SH, Shaahmadi F (2018) Mixed modified Fe_2O_3-WO_3 as new fuel borne catalyst (FBC) for biodiesel fuel. Energy 149:438–453. https://doi.org/10.1016/j.energy.2018.02.062
6. Debbarma S, Misra RD (2018) Effects of iron nanoparticle fuel additive on the performance and exhaust emissions of a compression ignition engine fueled with diesel and biodiesel. J Therm Sci Eng Appl 10(4). https://doi.org/10.1115/1.4038708
7. Bet-Moushoul E, Farhadi K, Mansourpanah Y, Nikbakht AM, Molaei R, Forough M (2016) Application of CaO-based/Au nanoparticles as heterogeneous nanocatalysts in biodiesel production. Fuel 164:119–127. https://doi.org/10.1016/j.fuel.2015.09.067
8. M. G€ U Ur€ U U, G. Gur Karakaya, D. Altıparmak, and A. Alıcılar, Improvement of diesel fuel properties by using additives. [Online]. Available: www.elsevier.com/locate/enconman
9. Kasper M, Sattler K, Siegmann RK, Matter SU, Siegmann HC (1999) The influence of fuel additives on the formation of carbon during combustion
10. Lissianski VV, Maly PM, Zamansky VM, Gardiner WC (2001) Utilization of iron additives for advanced control of NOx emissions from stationary combustion sources. Ind Eng Chem Res 40(15):3287–3293. https://doi.org/10.1021/ie010019q
11. Yu W, Xie H (2012) A review on nanofluids: preparation, stability mechanisms, and applications. J Nanomaterials 2012. https://doi.org/10.1155/2012/435873
12. Velusamy R, Kumar AS (2015) A review of nano additive in diesel. Artic J Chem Pharm Sci Available: https://www.researchgate.net/publication/282937905
13. Arul V, Selvan M, Anand RB, Udayakumar M (2009) Effects of cerium oxide nanoparticle addition in diesel and diesel-biodiesel-ethanol blends on the performance and emission characteristics of a CI engine. J Eng Appl Sci 4:7 Available: www.arpnjournals.com
14. Srinivas Rao D, Dash RK (2015) Effect of nanomaterials sizes on the dispersion stability of biodiesel based nanofluids. Adv Mater Lett 6(3):247–251. https://doi.org/10.5185/amlett.2015.5638
15. Jeong H (2011) The effect of voltage on a conductivity gradient in a nanochannel and its application to protein trapping. Macquarie 1:17–33. https://doi.org/10.1080/10408430701776680
16. Ortega G, Reguera E (2019) Biomedical applications of magnetite nanoparticles, no. 1. Elsevier Inc. https://doi.org/10.1016/B978-0-12-816913-1.00013-1
17. Mürbe J, Rechtenbach A, Töpfer J (2008) Synthesis and physical characterization of magnetite nanoparticles for biomedical applications. Mater Chem Phys 110(2–3):426–433. https://doi.org/10.1016/j.matchemphys.2008.02.037

18. Revia RA, Zhang M (2016) Magnetite nanoparticles for cancer diagnosis, treatment, and treatment monitoring: recent advances. Mater Today 19(3):157–168. https://doi.org/10.1016/j.mattod.2015.08.022
19. Nikitin A et al (2017) Synthesis, characterization and MRI application of magnetite water-soluble cubic nanoparticles. J Magn Magn Mater. 441:6–13. https://doi.org/10.1016/j.jmmm.2017.05.039
20. El-Gendy NS, Nassar HN (2021) Biosynthesized magnetite nanoparticles as an environmental opulence and sustainable wastewater treatment. Sci. Total Environ. 774:145610. https://doi.org/10.1016/j.scitotenv.2021.145610
21. Gao F (2019) An overview of surface-functionalized magnetic nanoparticles: preparation and application for wastewater treatment. ChemistrySelect 4(22):6805–6811. https://doi.org/10.1002/slct.201900701
22. Das C et al (2020) Green synthesis, characterization and application of natural product coated magnetite nanoparticles for wastewater treatment. Nanomaterials 10(8):1–19. https://doi.org/10.3390/nano10081615
23. Zhu H, Han J, Xiao JQ, Jin Y (2008) Uptake, translocation, and accumulation of manufactured iron oxide nanoparticles by pumpkin plants. J Environ Monit 10(6):713–717. https://doi.org/10.1039/b805998e
24. Rui M et al (2016) Iron oxide nanoparticles as a potential iron fertilizer for peanut (Arachis hypogaea). Front Plant Sci. 7:1–10. https://doi.org/10.3389/fpls.2016.00815
25. Sheykhbaglou R, Sedghi M, Shishevan MT, Sharifi RS (2010) Effects of nano-iron oxide particles on agronomic traits of soybean. Not Sci Biol. 2(2):112–113. https://doi.org/10.15835/nsb224667
26. Zhang Z et al (2021) The effects of Fe_2O_3 based DOC and SCR catalyst on the combustion and emission characteristics of a diesel engine fueled with biodiesel. Fuel 290:120039. https://doi.org/10.1016/j.fuel.2020.120039
27. Aalam CS, Saravanan DCG, Samath CM (2015) Reduction of diesel engine emissions using catalytic converter with nano aluminium oxide catalyst. Int J Res Emerg Sci Technol 2(7):17–22 Available: http://www.hindawi.com/journals/je/2013/589382/
28. Kaskun Ergani S, Kocaman A, Akinay Y (2021) Al_2O_3/SiO_2 nanoparticles-coated TiO_2 catalyst on the exhaust pollutants of a diesel engine. Appl Nanosci 11(12):2759–2766. https://doi.org/10.1007/s13204-021-02224-5
29. Jeong J-R, Lee S-J, Kim J-D, Shin S-C (2004) Magnetic properties of Fe_3O_4 nanoparticles encapsulated with poly (D, L lactide-Co-glycolide). Magn IEEE Trans 40(4):3015–3017. Available. https://doi.org/10.1023/A:1021231527095
30. Rashad MM, El-Sayed HM, Rasly M, Nasr MI (2012) Induction heating studies of magnetite nanospheres synthesized at room temperature for magnetic hyperthermia. J Magn Magn Mater 324(23):4019–4023. https://doi.org/10.1016/j.jmmm.2012.07.010
31. Aphesteguy JC, Kurlyandskaya GV, De Celis JP, Safronov AP, Schegoleva NN (2015) Magnetite nanoparticles prepared by co-precipitation method in different conditions. Mater Chem. Phys 161:243–249. https://doi.org/10.1016/j.matchemphys.2015.05.044
32. Valenzuela R et al (2009) Influence of stirring velocity on the synthesis of magnetite nanoparticles (Fe_3O_4) by the co-precipitation method. J Alloys Compd 488(1):227–231. https://doi.org/10.1016/j.jallcom.2009.08.087
33. Khalil MI (2015) Co-precipitation in aqueous solution synthesis of magnetite nanoparticles using iron(III) salts as precursors. Arab J Chem 8(2):279–284. Available. https://doi.org/10.1016/j.arabjc.2015.02.008
34. Togashi T, Umetsu M, Naka T, Ohara S, Hatakeyama Y, Adschiri T (2011) One-pot hydrothermal synthesis of an assembly of magnetite nanoneedles on a scaffold of cyclic-diphenylalanine nanorods. J Nanoparticle Res 13(9):3991–3999. https://doi.org/10.1007/s11051-011-0324-0
35. Gao G et al (2010) Solvothermal synthesis and characterization of size-controlled monodisperse Fe_3O_4 nanoparticles. J Mater Sci 45(13):3483–3489. https://doi.org/10.1007/s10853-010-4378-7
36. Asuha S, Suyala B, Siqintana X, Zhao S (2011) Direct synthesis of Fe_3O_4 nanopowder by thermal decomposition of Fe-urea complex and its properties. J Alloys Compd 509(6):2870–2873. https://doi.org/10.1016/j.jallcom.2010.11.145
37. Gao G et al (2010) Shape-controlled synthesis and magnetic properties of monodisperse Fe_3O_4 nanocubes. Cryst Growth Des 10(7):2888–2894. https://doi.org/10.1021/cg900920q
38. de Oliveira Guidolin T et al (2021) Photocatalytic pathway on the degradation of methylene blue from aqueous solutions using magnetite nanoparticles. J Clean Prod 318. https://doi.org/10.1016/j.jclepro.2021.128556
39. Niculescu AG, Chircov C, Grumezescu AM (2022) Magnetite nanoparticles: synthesis methods – a comparative review. Methods 199:16–27. https://doi.org/10.1016/j.ymeth.2021.04.018
40. Cabrera L, Gutierrez S, Menendez N, Morales MP, Herrasti P (2008) Magnetite nanoparticles: electrochemical synthesis and characterization. Electrochim Acta 53(8):3436–3441. https://doi.org/10.1016/j.electacta.2007.12.006
41. Basavegowda N, Baek KH (2021) Multimetallic nanoparticles as alternative antimicrobial agents: challenges and perspectives. Molecules 26(4). https://doi.org/10.3390/molecules26040912
42. Wallyn J, Anton N, Vandamme TF (2019) Synthesis, principles, and properties of magnetite nanoparticles for in vivo imaging applications—a review. Pharmaceutics 11(11). https://doi.org/10.3390/pharmaceutics11110601
43. James M, Revia RA, Stephen Z, Zhang M (2020) Microfluidic synthesis of iron oxide nanoparticles. Nanomaterials 10(11):1–19. https://doi.org/10.3390/nano10112113
44. Hu H et al (2010) Unique role of ionic liquid in microwave-assisted synthesis of monodisperse magnetite nanoparticles. Chem Commun 46(22):3866–3868. https://doi.org/10.1039/b927321b
45. Sirivat A, Paradee N (2019) Facile synthesis of gelatin-coated Fe_3O_4 nanoparticle: effect of pH in single-step co-precipitation for cancer drug loading. Mater Des 181. https://doi.org/10.1016/j.matdes.2019.107942
46. Salvador M, Gutiérrez G, Noriega S, Moyano A, Blanco-López MC, Matos M (2021) Microemulsion synthesis of superparamagnetic nanoparticles for bioapplications. Int J Mol Sci 22(1):1–17. https://doi.org/10.3390/ijms22010427
47. Rees WS, Muzzy JD, Liu M, Moore RL, McDowell DL (2005) A Multifunctional Approach To Development, Fabrication, And Characterization Of FE_3O_4 composites
48. Wu S et al (2011) Fe_3O_4 magnetic nanoparticles synthesis from tailings by ultrasonic chemical co-precipitation. Mater Lett. 65(12):1882–1884. https://doi.org/10.1016/j.matlet.2011.03.065
49. Wu W, He Q, Jiang C (2008) Magnetic iron oxide nanoparticles: synthesis and surface functionalization strategies. Nanoscale Res Lett 3(11):397–415. https://doi.org/10.1007/s11671-008-9174-9
50. Liu S, Yu B, Wang S, Shen Y, Cong H (2020) Preparation, surface functionalization and application of Fe_3O_4 magnetic nanoparticles. Adv Colloid Interface Sci 281. https://doi.org/10.1016/j.cis.2020.102165

51. Kumar S, Dinesha P, Bran I (2017) Influence of nanoparticles on the performance and emission characteristics of a biodiesel fuelled engine: an experimental analysis. Energy 140:98–105. https://doi.org/10.1016/j.energy.2017.08.079
52. Radwan MA, Rashad MA, Sadek MA, Elazab HA (2019) Synthesis, characterization and selected application of chitosan-coated magnetic iron oxide nanoparticles
53. Karthikeyan S, Prathima A (2016) Environmental effect on the impact of ferrofluid on Caulerpa Racemosa Oil methyl ester from marine macroalgae. Energy Sources, Part A Recover Util Environ Eff 38(21):3242–3248. https://doi.org/10.1080/15567036.2016.1143060
54. Aliramaji S, Zamanian A, Sohrabijam Z (2015) Characterization and synthesis of magnetite nanoparticles by innovative sonochemical method. Procedia Mater Sci 11:265–269. https://doi.org/10.1016/j.mspro.2015.11.022
55. Shen L et al (2014) Facile co-precipitation synthesis of shape-controlled magnetite nanoparticles. Ceram Int 40(1 PART B):1519–1524. https://doi.org/10.1016/j.ceramint.2013.07.037
56. Fadli A, Komalasari AA, Iwantono R, Addabsi AS (2019) Synthesis of magnetite nanoparticles via co-precipitation method, in IOP Conference Series. Mater Sci Eng 622(1). https://doi.org/10.1088/1757-899X/622/1/012013
57. Darwish MSA, Al-Harbi LM (2022) Self-heating properties of iron oxide nanoparticles prepared at room temperature via ultrasonic-assisted co-precipitation process. Soft Mater 20(1):35–44. https://doi.org/10.1080/1539445X.2021.1917425
58. Prabowo B, Khairunnisa T, Nandiyanto ABD (2018) Economic perspective in the production of magnetite (Fe_3O_4) nanoparticles by co-precipitation method. World Chem EngJ 2(2):1–4
59. Bui TQ, Ton SNC, Duong AT, Tran HT (2018) Size-dependent magnetic responsiveness of magnetite nanoparticles synthesised by co-precipitation and solvothermal methods. J Sci Adv Mater Devices 3(1):107–112. https://doi.org/10.1016/j.jsamd.2017.11.002
60. Radoń A, Drygała A, Hawełek Ł, Łukowiec D (2017) Structure and optical properties of Fe_3O_4 nanoparticles synthesized by co-precipitation method with different organic modifiers. Mater Charact 131:148–156. https://doi.org/10.1016/j.matchar.2017.06.034
61. Yuanbi Z, Zumin Q, Jiaying H (2008) Preparation and analysis of Fe_3O_4 magnetic nanoparticles used as targeted-drug carriers. Chinese J Chem Eng. 16(3):451–455
62. Mohammadi H, Nekobahr E, Akhtari J, Saeedi M, Akbari J, Fathi F (2021) Synthesis and characterization of magnetite nanoparticles by co-precipitation method coated with biocompatible compounds and evaluation of in-vitro cytotoxicity. Toxicol Reports 8:331–336. https://doi.org/10.1016/j.toxrep.2021.01.012
63. Jafari Eskandari M, Hasanzadeh I (2021) Size-controlled synthesis of Fe_3O_4 magnetic nanoparticles via an alternating magnetic field and ultrasonic-assisted chemical co-precipitation. Mater Sci Eng B Solid-State Mater Adv Technol 266:115050. https://doi.org/10.1016/j.mseb.2021.115050
64. Sulistyaningsih T, Santosa SJ, Siswanta D, Rusdiarso B (2017) Synthesis and characterization of magnetites obtained from mechanically and sonochemically assissted co-precipitation and reverse co-precipitation methods. Int J Mater Mech Manuf 5(1):16–19. https://doi.org/10.18178/ijmmm.2017.5.1.280
65. Nieciecka D, Cichy D (2022) Synthesis and characterization of magnetic drug carriers modified with Tb^{3+} ions
66. S. M. E. Sepasgozar, B. Feizyzadeh, A. Morsali, Q. Branch, Q. Branch, and M. Branch, Eco-friendly synthesis of magnetic iron oxide nanoparticles using achillea nobilis extract and evaluation of their antioxidant and antibacterial properties, 2022;12(2):61–71. doi: https://doi.org/10.30495/JFBT.2022.19330.
67. Jesus ACB et al (2020) Synthesis and magnetic interaction on concentrated Fe_3O_4 nanoparticles obtained by the co-precipitation and hydrothermal chemical methods. Ceram Int 46(8):11149–11153. https://doi.org/10.1016/j.ceramint.2020.01.135
68. O. Article, Applied biotechnology reports surface modification of superparamagnetic iron oxide nanoparticles by argon plasma for medical applications, 2022;9(1): 563–568. doi: https://doi.org/10.30491/JABR.2020.238608.1259.
69. Klencsár Z et al (2019) The effect of preparation conditions on magnetite nanoparticles obtained via chemical co-precipitation. Mater Chem Phys 223(2018):122–132. https://doi.org/10.1016/j.matchemphys.2018.10.049
70. Yazid NA, Joon YC (2019) Co-precipitation synthesis of magnetic nanoparticles for efficient removal of heavy metal from synthetic wastewater. AIP Conf Proc 2124. https://doi.org/10.1063/1.5117079
71. Al-Alawy AF, Al-Abod EE, Kadhim RM (2018) J. Eng 2019(16):2597–2603 Available: https://digital-library.theiet.org/content/journals/10.1049/joe.2018.8601
72. Saragi T, Depi BL, Butarbutar S, Permana B, Risdiana (2018) The impact of synthesis temperature on magnetite nanoparticles size synthesized by co-precipitation method. J Phys Conf Ser 1013. https://doi.org/10.1088/1742-6596/1013/1/012190
73. Yazdani F, Seddigh M (2016) Magnetite nanoparticles synthesized by co-precipitation method: the effects of various iron anions on specifications. Mater Chem Phys 184:318–323. https://doi.org/10.1016/j.matchemphys.2016.09.058
74. Kim JH, Kim SM, Il Kim Y (2014) Properties of magnetic nanoparticles prepared by co-precipitation. J Nanosci Nanotechnol 14(11):8739–8744. https://doi.org/10.1166/jnn.2014.9993
75. Mascolo MC, Pei Y, Ring TA (2013) Room temperature co-precipitation synthesis of magnetite nanoparticles in a large ph window with different bases. Materials (Basel). 6(12):5549–5567. https://doi.org/10.3390/ma6125549
76. Hariani PL, Faizal M, Ridwan R, Marsi M, Setiabudidaya D (2013) Synthesis and properties of Fe_3O_4 nanoparticles by co-precipitation method to removal procion dye. Int J Environ Sci Dev 4(3):336–340. https://doi.org/10.7763/ijesd.2013.v4.366
77. Petcharoen K, Sirivat A (2012) Synthesis and characterization of magnetite nanoparticles via the chemical co-precipitation method. Mater Sci Eng B Solid-State Mater Adv Technol 177(5):421–427. https://doi.org/10.1016/j.mseb.2012.01.003
78. Wei Y, Han B, Hu X, Lin Y, Wang X, Deng X (2012) Synthesis of Fe_3O_4 nanoparticles and their magnetic properties. Procedia Eng. 27(2011):632–637. https://doi.org/10.1016/j.proeng.2011.12.498
79. Ramadan W, Kareem M, Hannoyer B, Saha S (2011) Effect of pH on the structural and magnetic properties of magnetite nanoparticles synthesised by co-precipitation. Adv Mater Res 324:129–132. https://doi.org/10.4028/www.scientific.net/AMR.324.129

80. El Ghandoor H, Zidan HM, Khalil MMH, Ismail MIM (2012) Synthesis and some physical properties of magnetite (Fe_3O_4) nanoparticles. Int J Electrochem Sci 7(6):5734–5745
81. Parashar M, Shukla VK, Singh R (2020) Metal oxides nanoparticles via sol–gel method: a review on synthesis, characterization and applications. J Mater Sci Mater Electron 31(5):3729–3749. https://doi.org/10.1007/s10854-020-02994-8
82. Takai ZI, Mustafa MK, Asman S, Sekak KA (2019) Preparation and characterization of magnetite (Fe_3O_4) nanoparticles by sol-gel method
83. Marcelo G. A., Lodeiro C., Capelo J. L., Oliveira, E (2020) Magnetic, fluorescent and hybrid nanoparticles: from synthesis to application in biosystems. Mater Sci Eng C 106. https://doi.org/10.1016/j.msec.2019.110104
84. Piriyawong V, Thongpool V, Asanithi P, Limsuwan P (2012) Preparation and characterization of alumina nanoparticles in deionized water using laser ablation technique. J Nanomater 2012. https://doi.org/10.1155/2012/819403
85. Nee Koo K, Fauzi Ismail A, Othman MHD, Rahman MA, Sheng TZ (2019) Preparation and characterization of superparamagnetic magnetite (Fe_3O_4) nanoparticles: a short review
86. Shaker S, Zafarian S, Chakra CS, Rao KV (2013) Preparation and characterization of magnetite nanoparticles by sol-gel method for water treatment. Int J Innov Res Sci Eng Technol 2 [Online]. Available: www.ijirset.com
87. Suhel A, Abdul Rahim N, Abdul Rahman MR, Bin Ahmad KA (2021) Engine's behaviour on magnetite nanoparticles as additive and hydrogen addition of chicken fat methyl ester fuelled DICI engine: a dual fuel approach. Int J Hydrogen Energy 46(27):14824–14843. https://doi.org/10.1016/j.ijhydene.2021.01.219
88. Qi H, Yan B, Lu W, Li C, Yang Y (2011) A non-alkoxide sol-gel method for the preparation of magnetite (Fe_3O_4) nanoparticles. Curr Nanosci 7(3):381–388. https://doi.org/10.2174/157341311795542426
89. Lemine OM et al (2012) Sol-gel synthesis of 8 nm magnetite (Fe_3O_4) nanoparticles and their magnetic properties. Superlattices Microstruct 52(4):793–799. https://doi.org/10.1016/j.spmi.2012.07.009
90. Sundar S, Piraman S (2011) Nanospheres of Fe_3O_4 synthesis through sol-gel technique and their structural & magnetic characterization. Indian J Appl Res 3(7):123–126. https://doi.org/10.15373/2249555x/july2013/33
91. Zhao F, Zhang B, Feng L (2012) Preparation and magnetic properties of magnetite nanoparticles. Mater Lett 68(2):112–114. https://doi.org/10.1016/j.matlet.2011.09.116
92. Dissanayake DMSN, Mantilaka MMMGPG, Pitawala HMTGA (2020) Synthesis of low-cost magnetite nano-architectures from Sri Lankan laterites. J Geol Soc Sri Lanka 21(2):91. https://doi.org/10.4038/jgssl.v21i2.51
93. Basith NM et al (2016) Structural, magnetic, optical, and catalytic properties of Fe_3O_4 nanoparticles by the sol-gel method. J Supercond Nov Magn 29(8):2053–2058. https://doi.org/10.1007/s10948-016-3510-6
94. Hasanpour A, Niyaifar M, Asan M, Amighian J (2013) Synthesis and characterization of Fe_3O_4 and ZnO nanocomposites by the sol-gelmethod. J Magn Magn Mater 334:41–44. https://doi.org/10.1016/j.jmmm.2013.01.016
95. Hossain A, Sarker MSI, Khan MKR, Khan FA, Kamruzzaman M, Rahman MM (2018) Structural, magnetic, and electrical properties of sol–gel derived cobalt ferrite nanoparticles. Appl Phys A Mater Sci Process 124(9):1–7. https://doi.org/10.1007/s00339-018-2042-2
96. Hu P et al (2019) Temperature effects on magnetic properties of Fe_3O_4 nanoparticles synthesized by the sol-gel explosion-assisted method. J Alloys Compd 773:605–611. https://doi.org/10.1016/j.jallcom.2018.09.238
97. Akbar A, Yousaf H, Riaz S, Naseem S (2019) Role of precursor to solvent ratio in tuning the magnetization of iron oxide thin films – a sol-gel approach. J Magn Magn Mater 471:14–24. https://doi.org/10.1016/j.jmmm.2018.09.008
98. Eken AE, Ozenbas M (2009) Characterization of nanostructured magnetite thin films produced by sol-gel processing. J Sol-Gel Sci Technol 50(3):321–327. https://doi.org/10.1007/s10971-009-1971-9
99. Ou P, Xu G, Xu C, Zhang Y, Hou X, Han G (2010) Synthesis and characterization of magnetite nanoparticles by a simple solvothermal method
100. Aalam CS, Saravanan CG (2015) Performance enhancement of common-rail diesel engine using Al_2O_3 and Fe_3O_4 nanoparticles blended biodiesel. Int Res J Eng Technol Available: www.irjet.net
101. Kulkarni, S. A., Sawadh, P. S., & Kokate, K. K. (2012). Synthesis and characterization of Fe3O4 nanoparticles for engineering applications. In International Conference on Benchmarks in Engineering Science and Technology (ICBEST) (pp. 17–8).
102. Shafii MB, Daneshvar F, Jahani N, Mobini K (2011) Effect of ferrofluid on the performance and emission patterns of a four-stroke diesel engine. Adv Mech Eng 2011. https://doi.org/10.1155/2011/529049
103. Suhel A, Rahim NA, Rahman MRA, Bin Ahmad KA, Teoh YH, Abidin NZ (2021) An experimental investigation on the effect of ferrous ferric oxide nano-additive and chicken fat methyl ester on performance and emission characteristics of compression ignition engine. Symmetry (Basel) 13(2):1–23. https://doi.org/10.3390/sym13020265
104. Nouri M, Isfahani AHM, Shirneshan A (2021) Effects of Fe_2O_3 and Al_2O_3 nanoparticle-diesel fuel blends on the combustion, performance and emission characteristics of a diesel engine. Clean Technol Environ Policy 23(8):2265–2284. https://doi.org/10.1007/s10098-021-02134-8
105. Chaudhary V, Chaudhary R (2018) Magnetic nanoparticles: synthesis, functionalization, and applications
106. Aalam CS, Saravanan CG, Premanand B (2015) Influence of iron (II, III) oxide nanoparticles fuel additive on exhaust emissions and combustion characteristics of CRDI system assisted diesel engine. Int J Adv Eng Res Sci 2(3)
107. Ali HM, Babar H, Shah TR, Sajid MU, Qasim MA, Javed S (2018) Preparation techniques of TiO_2 nanofluids and challenges: a review. Appl Sci (Switzerland) 8(4). https://doi.org/10.3390/app8040587
108. Sandhya M, Ramasamy D, Sudhakar K, Kadirgama K, Harun WSW (2021) Ultrasonication an intensifying tool for preparation of stable nanofluids and study the time influence on distinct properties of graphene nanofluids – a systematic overview. Ultrasonics Sonochemistry 73. https://doi.org/10.1016/j.ultsonch.2021.105479
109. Devarajan Y, Munuswamy DB, Mahalingam A (2017) Performance, combustion and emission analysis on the effect of ferrofluid on neat biodiesel. Process Saf Environ Prot 111:283–291. https://doi.org/10.1016/j.psep.2017.07.021
110. Li X, Zhu D, Wang X (2007) Evaluation on dispersion behavior of the aqueous copper nano-suspensions. J Colloid Interface Sci 310(2):456–463. https://doi.org/10.1016/j.jcis.2007.02.067
111. Wei X, Wang L (2010) Synthesis and thermal conductivity of microfluidic copper nanofluids. Particuology 8(3):262–271. https://doi.org/10.1016/j.partic.2010.03.001

112. Kuo, K. K., Risha, G. A., Evans, B. J., & Boyer, E. (2003). Potential usage of energetic nano-sized powders for combustion and rocket propulsion. MRS Online Proceedings Library (OPL), 800.
113. Saxena V, Kumar N, Saxena VK (2017) A comprehensive review on combustion and stability aspects of metal nanoparticles and its additive effect on diesel and biodiesel fuelled C.I. engine. Renewable Sustainable Energy Rev 70:563–588. https://doi.org/10.1016/j.rser.2016.11.067
114. Singh AK, Raykar VS (2008) Microwave synthesis of silver nanofluids with polyvinylpyrrolidone (PVP) and their transport properties. Colloid Polym Sci 286(14–15):1667–1673. https://doi.org/10.1007/s00396-008-1932-9
115. Lee D, Kim JW, Kim BG (2006) A new parameter to control heat transport in nanofluids: surface charge state of the particle in suspension. J Phys Chem B 110(9):4323–4328. https://doi.org/10.1021/jp057225m
116. Vadasz P (2006) Heat conduction in nanofluid suspensions. J Heat Transfer 128(5):465–477. https://doi.org/10.1115/1.2175149
117. Daungthongsuk W, Wongwises S (2007) A critical review of convective heat transfer of nanofluids. Renewable Sustainable Energy Rev 11(5):797–817. https://doi.org/10.1016/j.rser.2005.06.005
118. Zhu H, Zhang C, Tang Y, Wang J, Ren B, Yin Y (2007) Preparation and thermal conductivity of suspensions of graphite nanoparticles. Carbon 45(1):226–228. https://doi.org/10.1016/j.carbon.2006.07.005
119. Hwang Y et al (2008) Production and dispersion stability of nanoparticles in nanofluids. Powder Technol 186(2):145–153. https://doi.org/10.1016/j.powtec.2007.11.020
120. Qiang AH, Zhao LM, Xu CJ, Zhou M (2007) Effect of dispersant on the colloidal stability of nano-sized CuO suspension. J Dispers Sci Technol 28(7):1004–1007. https://doi.org/10.1080/01932690701522293
121. Zhu D, Li X, Wang N, Wang X, Gao J, Li H (2009) Dispersion behavior and thermal conductivity characteristics of Al_2O_3-H_2O nanofluids. Curr Appl Phys 9(1):131–139. https://doi.org/10.1016/j.cap.2007.12.008
122. S. Mukherjee and S. Paria, Preparation and stability of nanofluids-a review. [Online]. Available: www.iosrjournals.org
123. Said Z et al (2015) Performance enhancement of a Flat Plate Solar collector using Titanium dioxide nanofluid and Polyethylene Glycol dispersant. J Clean Prod 92:343–353. https://doi.org/10.1016/j.jclepro.2015.01.007
124. Venkatachalapathy S, Kumaresan G, Suresh S (2015) Performance analysis of cylindrical heat pipe using nanofluids - an experimental study. Int J Multiph Flow 72:188–197. https://doi.org/10.1016/j.ijmultiphaseflow.2015.02.006
125. Hwang Y et al (2007) Stability and thermal conductivity characteristics of nanofluids. Thermochim Acta 455(1–2):70–74. https://doi.org/10.1016/j.tca.2006.11.036
126. Hwang Y, Park HS, Lee JK, Jung WH (2006) Thermal conductivity and lubrication characteristics of nanofluids. Curr Appl Phys 6(SUPPL. 1). https://doi.org/10.1016/j.cap.2006.01.014
127. Lee K, Hwang Y, Cheong S, Kwon L, Kim S, Lee J (2009) Performance evaluation of nano-lubricants of fullerene nanoparticles in refrigeration mineral oil. Curr Appl Phys 9(2 SUPPL). https://doi.org/10.1016/j.cap.2008.12.054
128. Gad MS, Abdel Razek SM, Manu PV, Jayaraj S (2021) Experimental investigations on diesel engine using alumina nanoparticle fuel additive. Adv Mech Eng 13(2). https://doi.org/10.1177/1687814020988402
129. Balamurugan S, Sajith V (2017) Experimental investigation on the stability and abrasive action of cerium oxide nanoparticles dispersed diesel. Energy 131:113–124. https://doi.org/10.1016/j.energy.2017.05.032
130. Seela CR, Ravisankar B (2018) Stability analysis and characterization of the nano emulsified Jatropha-curcas-based bio-fuel. Energy Sources Part A Recover Util Environ Eff 40(21):2564–2571. https://doi.org/10.1080/15567036.2018.1504143
131. Yu H, Hermann S, Schulz SE, Gessner T, Dong Z, Li WJ (2012) Optimizing sonication parameters for dispersion of single-walled carbon nanotubes. Chem Phys 408:11–16. https://doi.org/10.1016/j.chemphys.2012.08.020
132. Choudhary R, Khurana D, Kumar A, Subudhi S (2017) Stability analysis of Al_2O_3/water nanofluids. J Exp Nanosci 12(1):140–151. https://doi.org/10.1080/17458080.2017.1285445
133. Nasiri A, Shariaty-Niasar M, Rashidi A, Amrollahi A, Khodafarin R (2011) Effect of dispersion method on thermal conductivity and stability of nanofluid. Exp Therm Fluid Sci 35(4):717–723. https://doi.org/10.1016/j.expthermflusci.2011.01.006
134. Ruan B, Jacobi AM (2012) Ultrasonication effects on thermal and rheological properties of carbon nanotube suspensions. Nanoscale Res Lett 7. https://doi.org/10.1186/1556-276X-7-127
135. Leena M, Srinivasan S (2015) Synthesis and ultrasonic investigations of titanium oxide nanofluids. J Mol Liq 206:103–109. https://doi.org/10.1016/j.molliq.2015.02.001
136. Mondragon R, Julia JE, Barba A, Jarque JC (2012) Characterization of silica-water nanofluids dispersed with an ultrasound probe: a study of their physical properties and stability. Powder Technol 224:138–146. https://doi.org/10.1016/j.powtec.2012.02.043
137. Yusof SNA, Sidik NAC, Asako Y, Japar WMAA, Mohamed SB, Az Muhammad NM (2021) A comprehensive review of the influences of nanoparticles as a fuel additive in an internal combustion engine (ICE). Nanotechnol Rev 9(1):1326–1349. https://doi.org/10.1515/ntrev-2020-0104
138. Sumitomo S, Koizumi H, Uddin MA, Kato Y (2018) Comparison of dispersion behavior of agglomerated particles in liquid between ultrasonic irradiation and mechanical stirring. Ultrason Sonochem 40:822–831. https://doi.org/10.1016/j.ultsonch.2017.08.023
139. Elias MM et al (2014) Experimental investigation on the thermo-physical properties of Al_2O_3 nanoparticles suspended in car radiator coolant. Int Commun Heat Mass Transf 54:48–53. https://doi.org/10.1016/j.icheatmasstransfer.2014.03.005
140. Ouikhalfan M et al (2020) Stability and thermal conductivity enhancement of aqueous nanofluid based on surfactant-modified TiO_2. J Dispers Sci Technol 41(3):374–382. https://doi.org/10.1080/01932691.2019.1578665
141. Nabil MF, Azmi WH, Hamid KA, Mamat R (2018) Experimental investigation of heat transfer and friction factor of TiO_2-SiO_2 nanofluids in water:ethylene glycol mixture. Int J Heat Mass Transf 124:1361–1369. https://doi.org/10.1016/j.ijheatmasstransfer.2018.04.143
142. Hong KS, Hong TK, Yang HS (2006) Thermal conductivity of Fe nanofluids depending on the cluster size of nanoparticles. Appl Phys Lett 88(3):1–3. https://doi.org/10.1063/1.2166199

143. Amrollahi A, Hamidi AA, Rashidi AM (2008) The effects of temperature, volume fraction and vibration time on the thermo-physical properties of a carbon nanotube suspension (carbon nanofluid). Nanotechnology 19(31). https://doi.org/10.1088/0957-4484/19/31/315701
144. Chung SJ et al (2009) Characterization of ZnO nanoparticle suspension in water: Effectiveness of ultrasonic dispersion. Powder Technol 194(1–2):75–80. https://doi.org/10.1016/j.powtec.2009.03.025
145. El-Seesy AI, Attia AMA, El-Batsh HM (2018) The effect of aluminum oxide nanoparticles addition with Jojoba methyl ester-diesel fuel blend on a diesel engine performance, combustion and emission characteristics. Fuel 224:147–166. https://doi.org/10.1016/j.fuel.2018.03.076
146. Longo GA, Zilio C (2011) Experimental measurement of thermophysical properties of oxide-water nano-fluids down to ice-point. Exp Therm Fluid Sci 35(7):1313–1324. https://doi.org/10.1016/j.expthermflusci.2011.04.019
147. Parametthanuwat T, Rittidech S, Pattiya A (2010) A correlation to predict heat-transfer rates of a two-phase closed thermosyphon (TPCT) using silver nanofluid at normal operating conditions. Int J Heat Mass Transf 53(21–22):4960–4965. https://doi.org/10.1016/j.ijheatmasstransfer.2010.05.046
148. Sezer N, Atieh MA, Koç M (2019) A comprehensive review on synthesis, stability, thermophysical properties, and characterization of nanofluids. Powder Technol 344:404–431. https://doi.org/10.1016/j.powtec.2018.12.016
149. Shanbedi M, Zeinali Heris S, Maskooki A (2015) Experimental investigation of stability and thermophysical properties of carbon nanotubes suspension in the presence of different surfactants. J Therm Anal Calorim 120(2):1193–1201. https://doi.org/10.1007/s10973-015-4404-8
150. Tang QY, Shafiq I, Chan YC, Wong NB, Cheung R (2010) Study of the dispersion and electrical properties of carbon nanotubes treated by surfactants in dimethylacetamide. J Nanosci Nanotechnol 10(8):4967–4974. https://doi.org/10.1166/jnn.2010.2224
151. Li XF, Zhu DS, Wang XJ, Wang N, Gao JW, Li H (2008) Thermal conductivity enhancement dependent pH and chemical surfactant for Cu-H_2O nanofluids. Thermochim Acta 469(1–2):98–103. https://doi.org/10.1016/j.tca.2008.01.008
152. Bandyopadhyaya R, Nativ-Roth E, Regev O, Yerushalmi-Rozen R (2002) Stabilization of individual carbon nanotubes in aqueous solutions. Nano Lett 2(1):25–28. https://doi.org/10.1021/nl010065f
153. Xia G, Jiang H, Liu R, Zhai Y (2014) Effects of surfactant on the stability and thermal conductivity of Al_2O_3/de-ionized water nanofluids. Int J Therm Sci 84:118–124. https://doi.org/10.1016/j.ijthermalsci.2014.05.004
154. Sahooli M, Sabbaghi S, Shariaty Niassar M (2012) Preparation of CuO/water nanofluids using polyvinylpyrolidone and a survey on its stability and thermal conductivity
155. V. Kumar Nema and A. Singh, Emission reduction in a dual blend biodiesel fuelled CI engine using nano-fuel additives, 2018. Available: www.sciencedirect.comwww.materialstoday.com/proceedings2214-7853
156. Zhai YL, Xia GD, Liu XF, Li YF (2015) Heat transfer enhancement of Al_2O_3-H_2O nanofluids flowing through a micro heat sink with complex structure. Int Commun Heat Mass Transf 66:158–166. https://doi.org/10.1016/j.icheatmasstransfer.2015.05.025
157. Tiwari AK, Ghosh P, Sarkar J (2015) Particle concentration levels of various nanofluids in plate heat exchanger for best performance. Int J Heat Mass Transf 89:1110–1118. https://doi.org/10.1016/j.ijheatmasstransfer.2015.05.118
158. Kakati H, Mandal A, Laik S (2016) Promoting effect of Al_2O_3/ZnO-based nanofluids stabilized by SDS surfactant on CH_4+C_2H_6+C_3H_8 hydrate formation. J Ind Eng Chem 35:357–368. https://doi.org/10.1016/j.jiec.2016.01.014
159. Wen D, Lin G, Vafaei S, Zhang K (2009) Review of nanofluids for heat transfer applications. Particuology 7(2):141–150. https://doi.org/10.1016/j.partic.2009.01.007
160. Yarmand H et al (2015) Graphene nanoplatelets-silver hybrid nanofluids for enhanced heat transfer. Energy Convers Manag 100:419–428. https://doi.org/10.1016/j.enconman.2015.05.023
161. Zhang X, Gu H, Fujii M (2007) Effective thermal conductivity and thermal diffusivity of nanofluids containing spherical and cylindrical nanoparticles. Exp Therm Fluid Sci 31(6):593–599. https://doi.org/10.1016/j.expthermflusci.2006.06.009
162. Karthikeyan S, Elango A, Marimuthu P, Prathima A (2014) Performance, combustion and emission characteristic of a marine engine running on grape seed oil biodiesel blends with nano additive
163. D'Silva R, Binu KG, Bhat T (2015) Performance and emission characteristics of a C.I. engine fuelled with diesel and TiO_2 nanoparticles as fuel additive. Materials Today Proc 2(4–5):3728–3735. https://doi.org/10.1016/j.matpr.2015.07.162
164. Chen AF, Akmal Adzmi M, Adam A, Othman MF, Kamaruzzaman MK, Mrwan AG (2018) Combustion characteristics, engine performances and emissions of a diesel engine using nanoparticle-diesel fuel blends with aluminium oxide, carbon nanotubes and silicon oxide. Energy Convers Manag 171:461–477. https://doi.org/10.1016/j.enconman.2018.06.004
165. Gumus S, Ozcan H, Ozbey M, Topaloglu B (2016) Aluminum oxide and copper oxide nanodiesel fuel properties and usage in a compression ignition engine. Fuel 163:80–87. https://doi.org/10.1016/j.fuel.2015.09.048
166. Vedagiri P, Martin LJ, Varuvel EG, Subramanian T (2020) Experimental study on NO_x reduction in a grapeseed oil biodiesel-fueled CI engine using nanoemulsions and SCR retrofitment. Environ Sci Pollut Res 27(24):29703–29716. https://doi.org/10.1007/s11356-019-06097-8
167. Perumal V, Ilangkumaran M (2018) The influence of copper oxide nano particle added pongamia methyl ester biodiesel on the performance, combustion and emission of a diesel engine. Fuel 232:791–802. https://doi.org/10.1016/j.fuel.2018.04.129
168. Sahoo RR, Jain A (2019) Experimental analysis of nanofuel additives with magnetic fuel conditioning for diesel engine performance and emissions. Fuel 236:365–372. https://doi.org/10.1016/j.fuel.2018.09.027
169. Devarajan Y, Munuswamy DB, Mahalingam A (2019) Investigation on behavior of diesel engine performance, emission, and combustion characteristics using nano-additive in neat biodiesel. Heat Mass Transf und Stoffuebertragung 55(6):1641–1650. https://doi.org/10.1007/s00231-018-02537-2
170. Lenin MA, Swaminathan MR, Kumaresan G (2013) Performance and emission characteristics of a DI diesel engine with a nanofuel additive. Fuel 109:362–365. https://doi.org/10.1016/j.fuel.2013.03.042
171. Sajin JB, Pillai GO, Kesavapillai M, Varghese S (2021) Effect of nanoparticle on emission and performance characteristics of biodiesel. Int J Ambient Energy 42(13):1562–1568. https://doi.org/10.1080/01430750.2019.1611650

172. Praveena V, Martin MLJ, Geo VE (2020) Experimental characterization of CI engine performance, combustion and emission parameters using various metal oxide nanoemulsion of grapeseed oil methyl ester. J Therm Anal Calorim 139(6):3441–3456. https://doi.org/10.1007/s10973-019-08722-7
173. Tomar M, Kumar N (2020) Influence of nanoadditives on the performance and emission characteristics of a CI engine fuelled with diesel, biodiesel, and blends–a review. Energy Sources Part A Recover Util Environ Eff 42(23):2944–2961. https://doi.org/10.1080/15567036.2019.1623347
174. Venkata Ramanan M, Yuvarajan D (2016) Emission analysis on the influence of magnetite nanofluid on methyl ester in diesel engine. Atmos Pollut Res 7(3):477–481. https://doi.org/10.1016/j.apr.2015.12.001
175. Suhel A, Abdul Rahim N, Abdul Rahman MR, Bin Ahmad KA (2021) Improve direct injection compression ignition engine behavior using magnetite nano-fuel and hydrogen induction: a dual fuel approach. Energy Sources Part A Recover Util Environ Eff. https://doi.org/10.1080/15567036.2021.1946216
176. Kaliveer V, Basrithaya P, Nithesh, D'Almeida P, Kumar P, D'Silva R (2019) Effect of magnetite nanoadditive in waste cooking oil methyl ester on the performance and emission characteristics of CI engine. In: AIP Conference Proceedings, vol 2080. https://doi.org/10.1063/1.5092912
177. Yuvarajan D, Venkata Ramanan M (2016) Investigation on effect of magnetite nanofluid on performance and emission patterns of methyl esters of bio diesel. J Environ Eng Landsc Manag 24(2):90–96. https://doi.org/10.3846/16486897.2016.1142447
178. Devarajan Y, Venkata A, Madhavan R (2017) Emission analysis on the influence of ferrofluid on rice bran biodiesel
179. Yuvarajan D, Ramanan MV (2016) Effect of magnetite ferrofluid on the performance and emissions characteristics of diesel engine using methyl esters of mustard oil. Arab J Sci Eng 41(5):2023–2030. https://doi.org/10.1007/s13369-016-2060-3
180. S. Muthusamy, S. S. Nallathambi, R. Kumar Ramasamy, and S. T. Mohamed, Effects of nanoparticles blended biodiesel on single cylinder CI engine, in Materials Today: Proceedings, 2018;5(2):6831–6838. doi: https://doi.org/10.1016/j.matpr.2017.11.343.
181. Tyagi H, Phelan P, Prasher R (2007) Predicted efficiency of a nanofluid-based direct absorption solar receiver. In: Proceedings of the Energy Sustainability Conference 2007, pp 729–736. https://doi.org/10.1115/ES2007-36139
182. Prasher R, Bhattacharya P, Phelan PE (2006) Brownian-motion-based convective-conductive model for the effective thermal conductivity of nanofluids. J Heat Transfer 128(6):588–595. https://doi.org/10.1115/1.2188509
183. Krishnamurthy S, Bhattacharya P, Phelan PE, Prasher RS (2006) Enhanced mass transport in nanofluids. Nano Lett 6(3):419–423. https://doi.org/10.1021/nl0522532
184. Pivkina A, Ulyanova P, Frolov Y, Zavyalov S, Schoonman J (2004) Nanomaterials for heterogeneous combustion. Propellants Explos Pyrotech 29(1):39–48. https://doi.org/10.1002/prep.200400025
185. Hussain Vali R, Marouf Wani M (2020) Optimal utilization of ZnO nanoparticles blended diesel-water emulsion by varying compression ratio of a VCR diesel engine. J Environ Chem Eng 8(4). https://doi.org/10.1016/j.jece.2020.103884
186. Selvan VAM, Anand RB, Udayakumar M (2014) Effect of cerium oxide nanoparticles and carbon nanotubes as fuel-borne additives in diesterol blends on the performance, combustion and emission characteristics of a variable compression ratio engine. Fuel 130:160–167. https://doi.org/10.1016/j.fuel.2014.04.034
187. Ramachandran SB (2014) Ferrofluid-diesel blend. Int J Sci Res Publ 5(6) Available: www.ijsrp.org
188. Ranaware AA and Satpute ST, Correlation between effects of cerium oxide nanoparticles and ferrofluid on the performance and emission characteristics of a C.I. Engine. Available: www.iosrjournals.org
189. Sabet Sarvestany N, Farzad A, Ebrahimnia-Bajestan E, Mir M (2014) Effects of magnetic nanofluid fuel combustion on the performance and emission characteristics. J Dispers Sci Technol 35(12):1745–1750. https://doi.org/10.1080/01932691.2013.874296
190. Kishore NP, Gugulothu SK (2021) Effect of iron oxide nanoparticles blended concentration on performance, combustion and emission characteristics of CRDI diesel engine running on Mahua Methyl Ester Biodiesel
191. C. Syed Aalam, Investigation on the combustion and emission characteristics of CRDI diesel engine fuelled with nano Al_2O_3 and Fe_3O_4 particles blended biodiesel, in Materials Today: Proceedings, 2020;33:2540–2546. doi: https://doi.org/10.1016/j.matpr.2019.12.040.
192. Dhahad HA, Ali SAG (2019) Experimental study on the effect of nanoparticle addition on the pressure at the start of ignition, maximum pressure and timing of maximum pressure. ARPN J Eng Appl Sci 14(8):1478–1489
193. Nutakki PK, Gugulothu SK, Ramachander J, Sivasurya M (2022) Effect Of n-amyl alcohol/biodiesel blended nano additives on the performance, combustion and emission characteristics of CRDi diesel engine. Environ Sci Pollut Res 29(1):82–97. https://doi.org/10.1007/s11356-021-13165-5
194. Gad MS, Abdelghany ES (2020) Improving the combustion characteristics and emissions using nano titanium oxide additive to biodiesel, vol 03, pp 56–67
195. Anchupogu P, Rao LN, Banavathu B (2018) Effect of alumina nano additives into biodiesel-diesel blends on the combustion performance and emission characteristics of a diesel engine with exhaust gas recirculation. Environ Sci Pollut Res 25(23):23294–23306. https://doi.org/10.1007/s11356-018-2366-7
196. Characteristics E (2020) SS symmetry E ff ect of Nano-Graphene Oxide and n-Butanol Fuel Additives Blended with Diesel — Nigella sativa Biodiesel Fuel Emulsion on Diesel
197. Soudagar MEM et al (2020) An investigation on the influence of aluminium oxide nano-additive and honge oil methyl ester on engine performance, combustion and emission characteristics. Renew Energy 146:2291–2307. https://doi.org/10.1016/j.renene.2019.08.025
198. Saravanan N, Sasikumar KSK (2020) Engine combustion test using algae biofuel with nanofluid. J Sci Ind Res (India) 79(9):854–857
199. Yin Z, Hao J, Wei J (2021) Study on the influence of alumina nanomethanol fluid on the performance, combustion and emission of DMDF diesel engine. E3S Web Conf 268. https://doi.org/10.1051/e3sconf/202126801004

Publisher's Note

Springer Nature remains neutral with regard to jurisdictional claims in published maps and institutional affiliations.